AIMS Mathematics, 11(11): 37322–37354.
DOI: 10.3934/math.20261444
Received: 16 August 2026
Revised: 16 September 2026
Accepted: 18 September 2026
Published: 11 November 2026

https://www.aimspress.com/journal/Math

Research article

An exponentiated QLindley distribution: properties, inference, and applications

Sajadul Hussain[1], **Partha Jyoti Hazarika**[1], **Ankur Chakraborty**[1] **and Diego I. Gallardo**[2,*]

[1] Department of Statistics, Dibrugarh University, Assam, India

[2] Departamento de Estadística, Facultad de Ciencias, Universidad del Bío-Bío, Concepción, Chile

* **Correspondence:** Email: dgallardo@ubiobio.cl.

Abstract: The exponentiated-G family provides a convenient framework for introducing additional shape parameters into flexible lifetime distributions. In this study, we proposed a new two-parameter Exponentiated QLindley (EQL) distribution as an extension of the QLindley model. The proposed distribution exhibits a wide range of density and hazard rate shapes while retaining a tractable parametric structure, with the QLindley distribution obtained as the special case $\alpha = 1$. We derived several mathematical properties of the EQL distribution, including its quantile function, moments, generalized order statistics, reliability characteristics, and actuarial risk measures. We considered both classical and Bayesian estimation methods and conducted a comprehensive Monte Carlo simulation study to investigate their finite-sample performance under different parameter configurations and sample sizes. We illustrated the empirical applicability of the EQL model using four real datasets involving reliability, customer waiting times, air pollution in Delhi, India, and COVID-19 mortality in the Netherlands. We compared the proposed distribution with several well-known competing models using information criteria and goodness-of-fit statistics. The results showed that the EQL distribution provides a competitive, flexible alternative for modeling positive, right-skewed data, with the additional shape parameter significantly improving fit relative to the QLindley submodel in all four applications.

Keywords: exponentiated-G family; QLindley distribution; reliability analysis; parameter estimation; Bayesian inference; Monte Carlo simulation
Mathematics Subject Classification: 62E15, 62F10

1. Introduction

Lifetime and positive-valued data arise in a wide range of fields, including engineering, reliability, health sciences, actuarial science, hydrology, management, physics, computer science, and biological sciences. An important feature of such data is that their empirical distributions may exhibit substantial

skewness and different density and failure-rate patterns. As a result, although classical probability distributions remain useful in many applications, a single standard model may not adequately describe all observed data patterns. This has motivated the development of more flexible probability distributions obtained by introducing additional parameters or by applying suitable transformation and generalization mechanisms. Among the approaches proposed in the literature are various generalization and transformation mechanisms designed to increase the flexibility of classical distributions, including the Beta-G family [1], Weibull-G family [2], new alpha power transformed family [3], Teissier-G family [4], weighted cosine-G family [5], Type II exponentiated half logistic generated family [6], unit exponentiated half logistic power series family [7], Exponentiated power generalized Weibull power series family [8], and logarithmic-G family [9].

An important class of flexible models is obtained through exponentiation. Originally proposed as a distributional extension by Zacks [10], this approach introduces an additional parameter by raising the CDF of a baseline distribution to a positive power. The resulting exponentiated models can provide greater flexibility in the shape of the density and related functions while retaining the basic structure of the parent distribution. This construction has been widely investigated for different baseline distributions, including the exponentiated Weibull [11], exponentiated Ailamujia distribution [12], exponentiated Fréchet [13], exponentiated Gumbel [14], exponentiated Lindley [15], exponentiated Pareto [16], exponentiated Lomax [17], exponentiated Lindley geometric [18], exponentiated XLindley [19], exponentiated new XLindley [20], exponentiated ZLindley [21], and exponentiated modified Lindley [22]. These developments show that exponentiation provides a simple mechanism for extending parsimonious baseline distributions without discarding their original structure.

Within the class of parsimonious positive-valued distributions, Saaidia et al. [23] introduced the QLindley distribution, a one-parameter model derived from the affine exponential family. The QLindley distribution is of particular interest because it provides a simple alternative to other Lindley-type models and has been considered as a competitive alternative to the Lindley and XLindley distributions. Its probability density and cumulative distribution functions are given by

$$f(z;\theta) = \frac{\theta(1+\theta^2 z)e^{-\theta z}}{1+\theta}, \qquad z > 0, \quad \theta > 0,$$

and

$$F(z;\theta) = 1 - \frac{1+\theta+\theta^2 z}{1+\theta}e^{-\theta z}, \qquad z > 0, \quad \theta > 0,$$

respectively. Despite its useful properties, the QLindley distribution has only one parameter. Consequently, its ability to accommodate a wider range of distributional shapes of positive-valued data is inherently restricted by its parsimonious parameterization. This motivates the construction of a more flexible extension that preserves the analytical form of the QLindley model while introducing an additional shape parameter. The exponentiation technique provides a natural mechanism for this purpose. Specifically, if $G(x;\theta)$ denotes the QLindley cdf, we define

$$F(x;\alpha,\theta) = G(x;\theta)^{\alpha}, \qquad \alpha > 0, \quad \theta > 0.$$

The resulting model, referred to as the Exponentiated QLindley (EQL) distribution, retains the QLindley distribution as the special case $\alpha = 1$ while providing an additional degree of flexibility through α.

The proposed extension is motivated not only by distributional flexibility but also by the analytical tractability inherited from the QLindley baseline. In particular, the resulting EQL distribution admits an explicit quantile representation, which facilitates random variate generation and the evaluation of quantile-based reliability measures, while the additional shape parameter α provides greater flexibility in the density and hazard functions within the same distributional framework.

Although several exponentiated Lindley-type distributions have been introduced, the present EQL model is constructed from the QLindley baseline, a special case of the affine exponential family with $a(\theta) = 1$, $b(\theta) = \theta^2$, $c(\theta) = \theta$, as opposed to $a(\theta) = \theta$, $b(\theta) = 1$, $c(\theta) = \theta$ for the classical Lindley distribution. Consequently, the baseline hazard curvature differs from that of the classical Lindley distribution, and this distinction propagates through the exponentiation step to produce a distributional structure that is not shared by the different exponentiated Lindley-type models discussed above. In line with this structural distinction, our model exhibits a bathtub-shaped hazard for $0 < \alpha < 1$ and a monotonically increasing hazard for $\alpha \geq 1$ over the investigated parameter space. The EQL distribution therefore offers a tractable framework for capturing these two practically important lifetime behaviors: an initially high failure rate followed by improvement and subsequent deterioration (bathtub pattern), and a steadily increasing hazard characteristic of aging or wear-out effects.

In practical terms, α can therefore be interpreted as an index that distinguishes the dominant failure mechanism of the population under study. Values of α in $(0, 1)$ are appropriate for units or systems subject to early-life defects or infant-mortality-type failures that are gradually weeded out before the failure rate stabilizes and rises again, such as electronic components or newly commissioned mechanical systems. Values of $\alpha \geq 1$, by contrast, are appropriate for units whose failure rate increases steadily with age, reflecting cumulative wear, fatigue, or degradation, as is common in mechanical components under continuous stress or in biological aging processes. Rather than being a purely mathematical exponentiation parameter, α therefore carries a direct reliability interpretation: it identifies which of the two qualitatively different lifetime regimes-infant-mortality-dominated or wear-out-dominated, best describes the population being modeled, and its estimated value from data provides diagnostic information about the underlying failure mechanism.

These properties make the EQL distribution particularly useful in survival and reliability analysis, where it provides an effective framework for modeling components and systems in reliability engineering. Beyond reliability applications, the EQL distribution also proves valuable in analyzing waiting-time data, where it can capture the duration between successive events; in environmental studies, for modeling variables such as rainfall, pollutant concentration, or other positive-valued environmental measurements; and in mortality analysis, for describing lifetime and survival patterns across populations. Its ability to accommodate both bathtub-shaped and increasing hazard-rate behavior within a single tractable framework makes it a versatile and practically useful model for a broad range of positive-valued, right-skewed real-world datasets.

The main contributions of this study are as follows: First, we introduce the EQL distribution as a two-parameter extension of the QLindley model and establish its main distributional and reliability properties. Second, we investigate several classical estimation procedures, along with a Bayesian approach, and assess their finite-sample performance through a Monte Carlo simulation study. Third, we demonstrate the practical usefulness of the proposed model using four real datasets from different application areas, including reliability, customer waiting times, air pollution, and COVID-19 data. We compare the EQL model with several established competing distributions using likelihood-based

criteria and goodness-of-fit measures. Finally, since the QLindley distribution is nested within the EQL model at $\alpha = 1$, we employ a likelihood ratio test to assess whether the additional shape parameter provides a statistically significant improvement in model fit. Additional diagnostic plots, alternative estimation results, bootstrap confidence intervals, Bayesian convergence diagnostics, and further distributional, reliability, entropy, and actuarial results are provided in the Supplementary Material.

The remainder of the paper is organized as follows: Section 2 introduces the EQL distribution and presents its probability density and cumulative distribution functions. Section 3 presents the main distributional properties of the proposed model, while Section 4 discusses its principal reliability characteristics. Section 5 presents the classical and Bayesian estimation procedures considered in the study. Section 6 describes the Monte Carlo simulation study. Section 7 presents the applications to four real datasets and the corresponding model comparisons and inference. Finally, Section 8 concludes the paper.

2. The exponentiated QLindley distribution

Let $\mathcal{G}(x;\theta)$ denote the cumulative distribution function (CDF) of the QLindley distribution with parameter $\theta > 0$. We define the Exponentiated QLindley (EQL) distribution by applying a power transformation to $\mathcal{G}(x;\theta)$. Specifically, a random variable X is said to follow the EQL distribution, denoted by $X \sim \text{EQL}(\alpha,\theta)$, if its CDF is given by

$$F(x;\alpha,\theta) = [\mathcal{G}(x;\theta)]^{\alpha}, \qquad \alpha > 0, \quad \theta > 0, \quad x > 0, \tag{2.1}$$

where

$$\mathcal{G}(x;\theta) = 1 - \left(1 + \frac{\theta^2 x}{1+\theta}\right) e^{-\theta x}, \qquad x > 0, \quad \theta > 0. \tag{2.2}$$

Differentiating (2.1), the corresponding PDF is

$$f(x;\alpha,\theta) = \frac{\alpha\theta(1+\theta^2 x)}{1+\theta} e^{-\theta x} [\mathcal{G}(x;\theta)]^{\alpha-1}, \qquad x > 0, \tag{2.3}$$

where α is the additional shape parameter introduced by the exponentiation mechanism, while θ is the positive parameter inherited from the QLindley distribution.

An important property of the proposed model is that it contains the QLindley distribution as a special case. In fact, setting $\alpha = 1$ in (2.1) gives

$$F(x;1,\theta) = \mathcal{G}(x;\theta),$$

and therefore, $X \sim \text{EQL}(1,\theta) \equiv \text{QL}(\theta)$. Thus, the parameter α controls the departure from the baseline QLindley model, while θ retains the role of the original QLindley parameter. This nested structure will also be useful for comparing the EQL and QLindley models through likelihood-based inference.

Figure 1 illustrates the shapes of the EQL density for different combinations of α and θ. The figure shows that varying these parameters allows the model to accommodate different density shapes, including decreasing and unimodal forms. In particular, the additional parameter α provides flexibility beyond that available under the one-parameter QLindley model. These different density shapes make the EQL distribution a flexible candidate for modeling positive-valued and lifetime data.

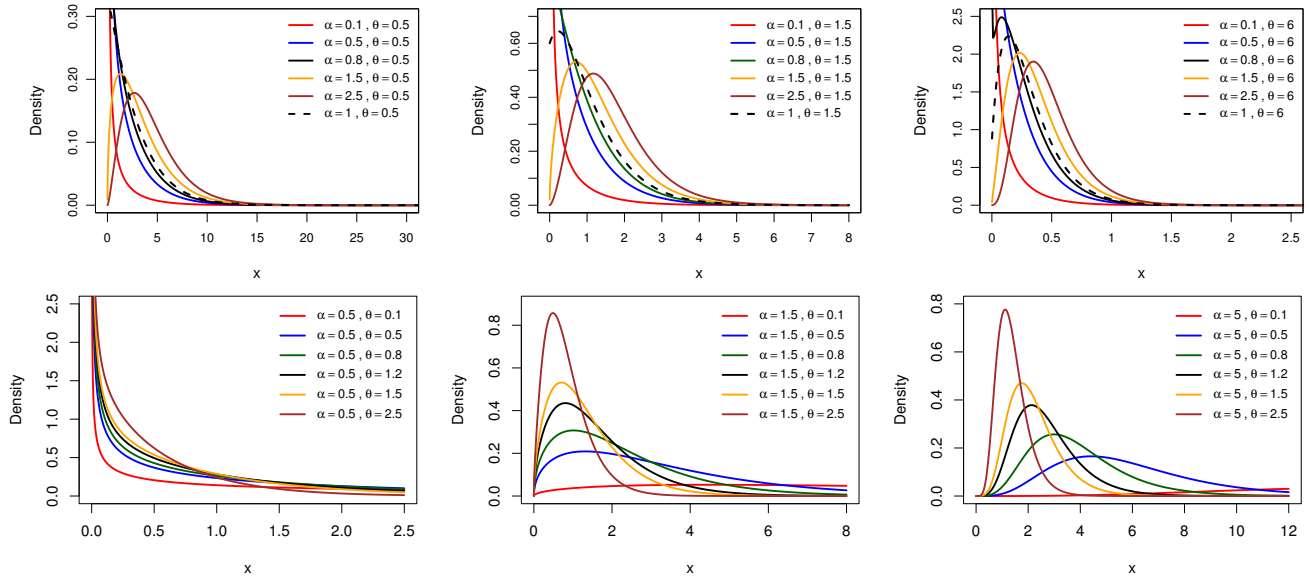


Figure 1. Density shapes of the EQL distribution for selected combinations of the parameters α and θ.

3. Statistical properties

In this section, we present selected statistical properties of the EQL distribution, focusing on the quantile function and random generation, moments, and mode.

3.1. Quantile function and random generation

The EQL distribution admits a closed-form quantile function in terms of the Lambert W function, which is also useful for random variate generation.

Proposition 1. For $0 < p < 1$, the quantile function of the EQL distribution is given by

$$Q(p) = -\frac{1+\theta}{\theta^2} - \frac{1}{\theta} W_{-1}\left[-\frac{1+\theta}{\theta}\left(1 - p^{1/\alpha}\right) e^{-(1+\theta)/\theta}\right]. \tag{3.1}$$

Here, $W_{-1}(\cdot)$ denotes the lower real branch of the Lambert W function.

Proof. Setting $F(x;\alpha,\theta) = p$ in (2.1) gives

$$\left(1 + \frac{\theta^2 x}{1+\theta}\right) e^{-\theta x} = 1 - p^{1/\alpha}.$$

Letting $y = 1 + \theta^2 x/(1+\theta)$, and applying the definition of the Lambert W function yields

$$x = -\frac{1+\theta}{\theta^2} - \frac{1}{\theta} W_{-1}\left[-\frac{1+\theta}{\theta}\left(1 - p^{1/\alpha}\right) e^{-(1+\theta)/\theta}\right],$$

which proves (3.1). □

Remark 1. The argument of the Lambert W function in (3.1) is $w = -qte^{-t}$, where $t = (1+\theta)/\theta > 1$ and $q = 1 - p^{1/\alpha} \in (0,1)$. Since $t > 1$ implies $te^{-t} \in (0, e^{-1})$, we have $w \in (-1/e, 0)$ for all $0 < p < 1$, $\alpha > 0$, and $\theta > 0$. Thus, both real branches W_0 and W_{-1} are defined. From the transformation $y = 1 + \theta^2 x/(1+\theta)$, we have $W(w) = -ty$. Since $x > 0$ requires $y > 1$, an admissible quantile must satisfy $W(w) < -t < -1$. The principal branch has $W_0(w) \in (-1, 0)$ and therefore cannot yield a positive solution. On the other hand, $0 < q < 1$ gives $w > -te^{-t}$, and since ze^z is decreasing on $(-\infty, -1)$, $W_{-1}(w) < -t$. Hence, W_{-1} is the unique real branch yielding an admissible positive solution, and it is used throughout the random-number generation and simulation study.

The first quartile, median, and third quartile are obtained directly from (3.1) as

$$Q_1 = Q(1/4), \qquad Q_2 = Q(1/2), \qquad \text{and} \qquad Q_3 = Q(3/4).$$

Figure 2 illustrates the behavior of these quartiles for different combinations of α and θ, highlighting the effects of the model parameters on the location and dispersion of the distribution.

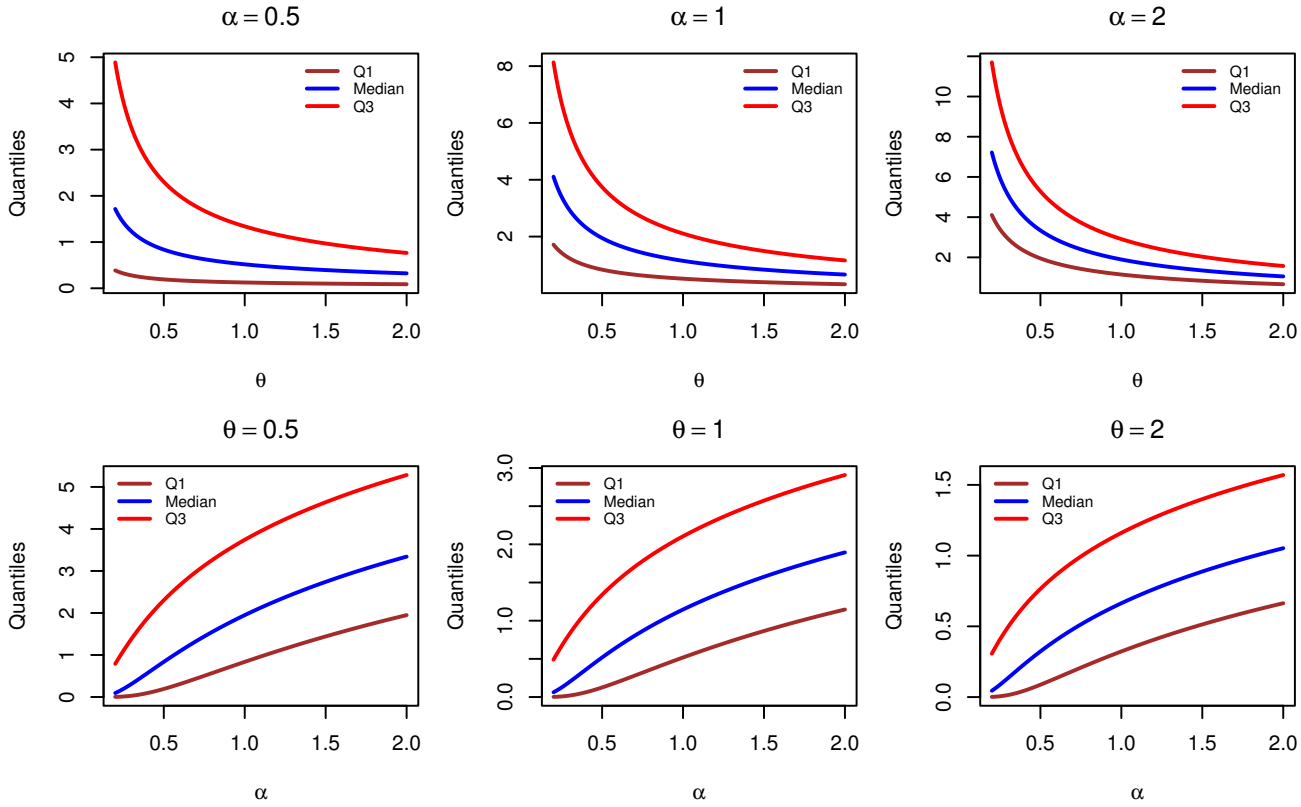


Figure 2. First quartile, median, and third quartile of the EQL distribution for different combinations of α and θ.

The closed-form quantile function also provides a direct method for generating random variates. Specifically, if $U \sim U(0,1)$, then $X = Q(U)$ follows the EQL distribution. Thus, random samples can be generated using the inverse-transform method summarized in Algorithm 1.

Algorithm 1. Generation of random samples from the EQL distribution.

1: **Input:** Sample size n, parameters $\alpha > 0$ and $\theta > 0$
2: **Output:** Random sample $\{X_1, \ldots, X_n\}$ from the EQL distribution
3: **for** $i = 1, \ldots, n$ **do**
4: Generate $U_i \sim U(0, 1)$
5: Set $X_i = Q(U_i)$, where $Q(\cdot)$ is given in (3.1)
6: **end for**
7: **return** $\{X_1, \ldots, X_n\}$

3.2. Moments

The raw moments provide useful measures for characterizing the location and dispersion of the EQL distribution. The following proposition gives a general expression for the r-th ordinary moment.

Proposition 2. Let $X \sim EQL(\alpha, \theta)$. For $r \geq 0$, the r-th ordinary moment $\mu'_r = E(X^r)$ is given by

$$\begin{aligned} \mu'_r = \frac{\alpha\theta}{1+\theta} \sum_{k=0}^{\infty} (-1)^k \binom{\alpha-1}{k} \sum_{j=0}^{k} \binom{k}{j} \left(\frac{\theta^2}{1+\theta}\right)^j \\ \times \left[\frac{\Gamma(r+j+1)}{[(k+1)\theta]^{r+j+1}} + \theta^2 \frac{\Gamma(r+j+2)}{[(k+1)\theta]^{r+j+2}} \right]. \end{aligned} \tag{3.2}$$

The first two moments provide the mean and variance according to

$$E(X) = \mu'_1, \qquad \text{and} \qquad \text{Var}(X) = \mu'_2 - (\mu'_1)^2. \tag{3.3}$$

Higher-order moments can be used to obtain the skewness, kurtosis, and coefficient of variation. The proof of Proposition 2, including the convergence of the resulting infinite series, is provided in Section S1.1 of the Supplementary Material.

To further validate the derived raw-moment expression numerically, the first three raw moments were evaluated for several representative combinations of α and θ and compared with the corresponding values obtained through direct numerical integration of the EQL density. The analytical and numerical results showed excellent agreement across all considered parameter combinations, with very small relative errors. This close agreement provides numerical confirmation of the accuracy of the derived moment expression. The complete numerical verification results are reported in Table S1 of the Supplementary Material.

3.3. Mode

The mode of the EQL distribution is obtained by solving

$$\frac{d}{dx} \log f(x; \alpha, \theta) = 0.$$

For the EQL distribution, this condition can be written as

$$\mathcal{G}(x; \theta) \left(\frac{\theta^2}{1+\theta^2 x} - \theta \right) - (\alpha - 1) e^{-\theta x} \left[\frac{\theta^2}{1+\theta} - \theta \left(1 + \frac{\theta^2 x}{1+\theta} \right) \right] = 0. \tag{3.4}$$

The mode does not admit a closed-form expression and can therefore be obtained numerically from Eq (3.4). Additional properties, including incomplete moments, Bonferroni and Lorenz curves, and generalized order statistics, are provided in the Supplementary Material S1.

4. Lifetime reliability measures

This section presents the main lifetime reliability characteristics of the proposed EQL distribution. We derive the survival, hazard, and reversed hazard rate functions and discuss several additional reliability measures, including the mean inactivity time, mean residual life, reliability aging intensity, and stress–strength reliability.

4.1. Survival and hazard rate functions

The survival function represents the probability that a system, individual, or component survives beyond a specified time x. From Eq (2.1), the survival function of the EQL distribution is

$$S(x;\alpha,\theta) = 1 - F(x;\alpha,\theta) = 1 - [\mathcal{G}(x;\theta)]^{\alpha}. \tag{4.1}$$

The hazard rate function describes the instantaneous risk of failure at time x, conditional on survival up to that time. For the EQL distribution, it is given by

$$h(x;\alpha,\theta) = \frac{\alpha g(x;\theta)\,[\mathcal{G}(x;\theta)]^{\alpha-1}}{1-[\mathcal{G}(x;\theta)]^{\alpha}}, \qquad x > 0, \tag{4.2}$$

where

$$g(x;\theta) = \frac{\theta(1+\theta^2 x)}{1+\theta} e^{-\theta x}.$$

The reversed hazard rate, which is useful for characterizing the behavior of the distribution near its lower tail, is

$$r(x;\alpha,\theta) = \frac{f(x;\alpha,\theta)}{F(x;\alpha,\theta)} = \frac{\alpha\theta(1+\theta^2 x)}{1+\theta}\frac{e^{-\theta x}}{\mathcal{G}(x;\theta)}, \qquad x > 0. \tag{4.3}$$

4.2. Asymptotic and numerical characterization of the hazard rate

To further investigate the hazard-rate behavior of the EQL distribution, we examine its limiting behavior and the sign of its first derivative. Using the expansion of $\mathcal{G}(x;\theta)$ around $x = 0$, we obtain

$$\mathcal{G}(x;\theta) = \frac{\theta}{1+\theta}x + O(x^2), \tag{4.4}$$

and hence

$$h(x;\alpha,\theta) \sim \alpha\left(\frac{\theta}{1+\theta}\right)^{\alpha} x^{\alpha-1}, \qquad x \to 0^+.$$

Therefore,

$$\lim_{x\to 0^+} h(x;\alpha,\theta) = \begin{cases} \infty, & 0 < \alpha < 1, \\ \dfrac{\theta}{1+\theta}, & \alpha = 1, \\ 0, & \alpha > 1. \end{cases} \tag{4.5}$$

Moreover, since $\mathcal{G}(x;\theta) \to 1$ and $1 - \mathcal{G}(x;\theta)^{\alpha} \sim \alpha[1 - \mathcal{G}(x;\theta)]$ as $x \to \infty$, a direct substitution into $h(x;\alpha,\theta) = \alpha\mathcal{G}(x;\theta)^{\alpha-1}g(x;\theta)/[1 - \mathcal{G}(x;\theta)^{\alpha}]$ gives

$$h(x;\alpha,\theta) \sim \frac{\theta(1+\theta^2 x)}{1+\theta+\theta^2 x} \longrightarrow \theta, \qquad x \to \infty.$$

Thus,

$$\lim_{x\to\infty} h(x;\alpha,\theta) = \theta, \qquad \text{for every } \alpha > 0,\ \theta > 0. \tag{4.6}$$

For monotonicity, logarithmic differentiation gives

$$\frac{h'(x;\alpha,\theta)}{h(x;\alpha,\theta)} = \frac{\theta^2}{1+\theta^2 x} - \theta + (\alpha-1)\frac{g(x;\theta)}{\mathcal{G}(x;\theta)} + h(x;\alpha,\theta). \tag{4.7}$$

Since $h(x;\alpha,\theta) > 0$, the sign of $h'(x;\alpha,\theta)$ is determined by the right-hand side of (4.7).

For $\alpha = 1$, the hazard function reduces to

$$h(x;1,\theta) = \frac{\theta(1+\theta^2 x)}{1+\theta+\theta^2 x},$$

with

$$h'(x;1,\theta) = \frac{\theta^4}{(1+\theta+\theta^2 x)^2} > 0, \qquad x > 0,\ \theta > 0. \tag{4.8}$$

Hence the hazard rate is strictly increasing when $\alpha = 1$.

A systematic numerical evaluation of (4.7) was then performed over a 100×100 grid of parameter combinations, with $0.05 \le \alpha, \theta \le 5$ and increment 0.05. All 1,900 combinations with $0 < \alpha < 1$ showed one sign change of h' from negative to positive, indicating an initially decreasing hazard followed by an increase toward θ, and hence a bathtub-shaped hazard rate. For all 8,100 combinations with $\alpha \ge 1$, $h'(x) > 0$ throughout the investigated range, indicating a monotonically increasing hazard rate. No globally decreasing or upside-down-bathtub hazard patterns were detected. An independent finite-difference evaluation of $h'(x)$ gave the same classification.

Thus, over the investigated parameter space, the EQL distribution exhibits

$$0 < \alpha < 1 : \text{ bathtub-shaped}, \qquad \alpha \ge 1 : \text{ increasing}.$$

Figure 3 presents the hazard rate functions of the EQL distribution for selected combinations of α and θ. For $0 < \alpha < 1$, the hazard rate initially decreases and subsequently increases toward its limiting value θ, resulting in a bathtub-shaped pattern. For $\alpha \ge 1$, the hazard rate is increasing toward θ. Thus, the figure illustrates the two principal hazard-rate behaviors identified by the systematic numerical analysis: a bathtub-shaped hazard for $0 < \alpha < 1$ and an increasing hazard for $\alpha \ge 1$. The curves shown are representative of the general classification obtained from the numerical evaluation of the hazard-rate derivative.

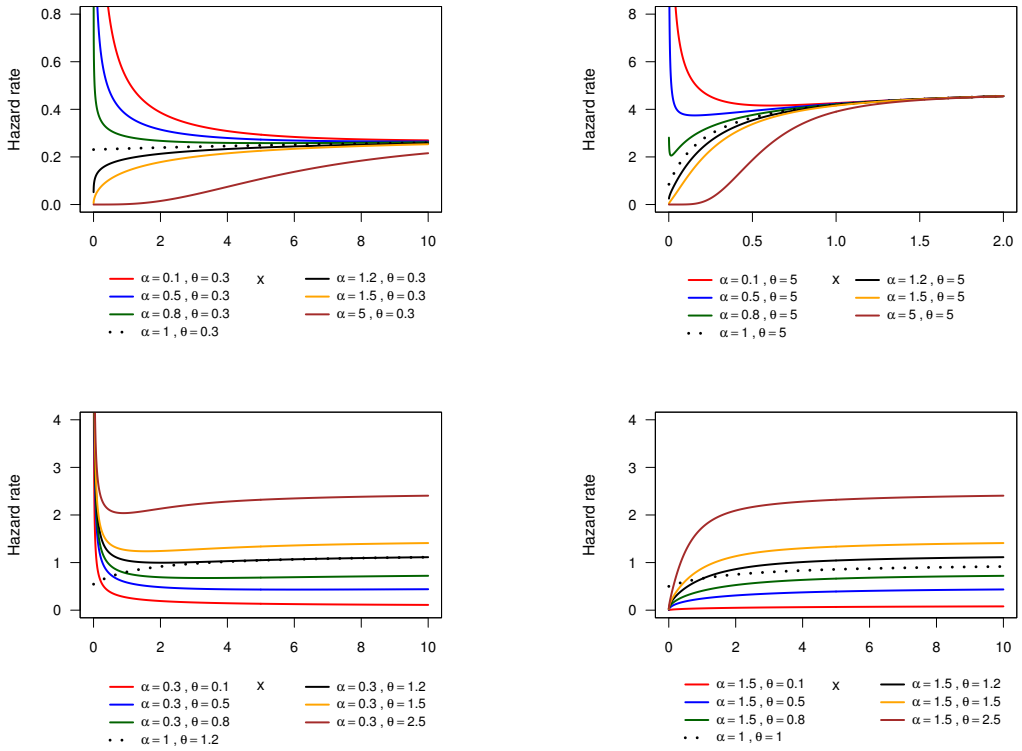


Figure 3. Hazard rate functions of the EQL distribution for selected combinations of α and θ.

4.3. Mean inactivity time and mean residual life

Two complementary measures of lifetime behavior are the mean inactivity time (MIT) and the mean residual life (MRL). The MIT function measures the expected time elapsed since failure, conditional on failure having occurred before time t, whereas the MRL function measures the expected remaining lifetime conditional on survival beyond t.

The MIT function is defined by

$$\mathrm{MIT}(t) = E(t - X \mid X \le t) = \frac{1}{F(t)} \int_0^t F(x)\, dx, \qquad t > 0. \tag{4.9}$$

For the EQL distribution, we can obtain a series representation of the MIT function from the CDF. Its explicit expression is provided in Section S2 of the Supplementary Material.

The MRL function is defined as

$$\mathrm{MRL}(t) = E(X - t \mid X > t) = \frac{1}{S(t)} \int_t^\infty S(x)\, dx, \qquad t > 0. \tag{4.10}$$

For the EQL model, the corresponding analytical expression in terms of incomplete gamma functions is also provided in Section S2 of the Supplementary Material.

Numerical evaluations of the MIT and MRL functions for different combinations of α and θ are presented in Section S2. The corresponding plots illustrate the behavior of these two complementary lifetime measures and show that the EQL model can accommodate different patterns of past and future lifetime behavior.

4.4. Reliability aging intensity

The reliability aging intensity (RAI) function provides a useful measure for characterizing the local aging behavior of a lifetime distribution by quantifying the rate of change of its hazard function with respect to x. Following recent use of this measure in the reliability literature (see, e.g., Elbarougy et al. [24]), the RAI function is defined as the logarithmic derivative of the hazard rate,

$$\mathrm{RAI}(x) = \frac{d}{dx}\log h(x;\alpha,\theta) = \frac{h'(x;\alpha,\theta)}{h(x;\alpha,\theta)}, \qquad x > 0. \tag{4.11}$$

It should be noted that this quantity is distinct from the aging intensity function $L(x) = xh(x)/H(x)$, where $H(x) = -\log S(x)$ denotes the cumulative hazard function, introduced by Jiang et al. [25] and widely used in the reliability literature. The function $L(x)$ compares the instantaneous hazard rate to its running average over $(0, x]$ and is classified relative to the threshold value 1, whereas $\mathrm{RAI}(x)$ in (4.11) is classified relative to 0 and directly captures the local rate of change of $h(x;\alpha,\theta)$.

For the EQL distribution, the RAI function can be shown to take the form

$$\mathrm{RAI}(x) = \frac{\theta^2}{1+\theta^2 x} - \theta + (\alpha-1)\frac{\mathcal{G}'(x;\theta)}{\mathcal{G}(x;\theta)} + \frac{\alpha[\mathcal{G}(x;\theta)]^{\alpha-1}\mathcal{G}'(x;\theta)}{1-[\mathcal{G}(x;\theta)]^{\alpha}}, \qquad x > 0. \tag{4.12}$$

As $\mathrm{RAI}(x)$ represents the logarithmic derivative of the hazard function $h(x;\alpha,\theta)$, its sign describes the local direction of change of the hazard rate. Specifically, $\mathrm{RAI}(x) > 0$ indicates that $h(x;\alpha,\theta)$ is locally increasing, whereas $\mathrm{RAI}(x) < 0$ indicates that it is locally decreasing. A global classification requires the corresponding sign condition to hold throughout the support. Thus, $\mathrm{RAI}(x) \geq 0$ for all $x > 0$ implies that the distribution has an increasing failure rate (IFR), whereas $\mathrm{RAI}(x) \leq 0$ for all $x > 0$ implies a decreasing failure rate (DFR). If $\mathrm{RAI}(x)$ changes sign at some x_0, the hazard rate is non-monotone. In particular, a change from negative to positive at x_0 identifies x_0 as a local minimum of the hazard rate, corresponding to a bathtub-shaped behavior, whereas a change from positive to negative identifies a local maximum, corresponding to an upside-down bathtub-shaped behavior. Therefore, for non-monotone hazard functions, $\mathrm{RAI}(x)$ is more appropriately interpreted as a measure for identifying the local direction and turning points of the hazard rate rather than as evidence of a single global aging class.

Consequently, the RAI function, together with its sign pattern in (4.12), provides a convenient characterization of the aging behavior of the EQL distribution across different combinations of (α,θ), encompassing both increasing and decreasing hazard-rate regimes and, where applicable, non-monotone hazard-rate patterns. Further numerical results illustrating the hazard rate, RAI function, and corresponding aging classifications for selected parameter configurations are provided in Supplementary Material S2.3.

4.5. Stress–strength reliability

The stress–strength reliability represents the probability that the strength of a system exceeds the applied stress,

$$\mathcal{R} = P(U > V),$$

where U and V denote independent random variables representing the strength and stress, respectively.

Case 1: Common baseline parameter θ.

Let $U \sim \text{EQL}(\alpha_1, \theta)$ and $V \sim \text{EQL}(\alpha_2, \theta)$ be independent, with a common value of θ. Then

$$\mathcal{R} = P(U > V) = \int_0^\infty S_U(v) f_V(v)\, dv = \int_0^\infty \{1 - [\mathcal{G}(v;\theta)]^{\alpha_1}\} \frac{\alpha_2\theta(1+\theta^2 v)}{1+\theta} e^{-\theta v} [\mathcal{G}(v;\theta)]^{\alpha_2 - 1}\, dv. \quad (4.13)$$

Since $d\mathcal{G}(v;\theta) = \dfrac{\theta(1+\theta^2 v)}{1+\theta} e^{-\theta v}\, dv$, the substitution $u = \mathcal{G}(v;\theta)$ reduces (4.13) to

$$\mathcal{R} = \alpha_2 \int_0^1 (1 - u^{\alpha_1}) u^{\alpha_2 - 1}\, du = \frac{\alpha_1}{\alpha_1 + \alpha_2}, \quad (4.14)$$

so that under the common-θ specification, $\mathcal{R}$ depends only on the shape parameters α_1, α_2, with θ cancelling entirely. This is a special case of a Lehmann-type alternative, since $\mathcal{G}(v;\theta)$ enters (4.13) only through the change of variable $u = \mathcal{G}(v;\theta) \in (0,1)$. The value $\mathcal{R} = 1/2$ is obtained *only* in the symmetric case $\alpha_1 = \alpha_2$; more generally, $\mathcal{R} > 1/2$ when $\alpha_1 > \alpha_2$ (strength tends to exceed stress) and $\mathcal{R} < 1/2$ when $\alpha_1 < \alpha_2$.

Case 2: Distinct baseline parameters $\theta_1 \neq \theta_2$.

The common-θ assumption above is restrictive, requiring strength and stress to share the same scale behavior. In the more general and practically relevant setting $U \sim \text{EQL}(\alpha_1, \theta_1)$, $V \sim \text{EQL}(\alpha_2, \theta_2)$ with $\theta_1 \neq \theta_2$,

$$\mathcal{R} = \int_0^\infty \{1 - [\mathcal{G}(v;\theta_1)]^{\alpha_1}\} f(v;\alpha_2,\theta_2)\, dv. \quad (4.15)$$

Here the substitution $u = \mathcal{G}(v;\theta_2)$ no longer removes θ_1 from the surviving term $[\mathcal{G}(v;\theta_1)]^{\alpha_1}$, since $\mathcal{G}(\cdot;\theta_1)$ and $\mathcal{G}(\cdot;\theta_2)$ are not related by a common monotone transformation when $\theta_1 \neq \theta_2$. Consequently, (4.15) does not admit a closed form in general, and $\mathcal{R}$ must be evaluated numerically (e.g., by adaptive quadrature) for given $(\alpha_1, \theta_1, \alpha_2, \theta_2)$. Table 1 reports $\widehat{\mathcal{R}}$ for representative parameter combinations; the common-θ rows agree with Eq (4.14), confirming the numerical procedure, while the $\theta_1 \neq \theta_2$ rows illustrate that $\mathcal{R}$ then depends on the scale parameters as well.

Table 1. Numerically evaluated stress–strength reliability $\mathcal{R} = P(U > V)$ for $U \sim \text{EQL}(\alpha_1, \theta_1)$, $V \sim \text{EQL}(\alpha_2, \theta_2)$.

α_1	θ_1	α_2	θ_2	$\widehat{\mathcal{R}}$
1.0	1.5	1.0	1.5	$0.5000^\dagger$
2.0	1.5	1.0	1.5	$0.6667^\dagger$
1.0	1.5	2.0	1.5	$0.3333^\dagger$
2.0	1.0	1.0	2.5	0.8709
1.0	0.5	2.0	2.5	0.7258

*Note: Common-θ cases.

Additional results related to uncertainty quantification and risk assessment are also provided in the Supplementary Material. In particular, we derive Rényi and Shannon entropy measures to quantify the uncertainty associated with the EQL distribution, and we obtain several actuarial risk measures,

including the limited expected value, value-at-risk (VaR), tail value-at-risk (TVaR), and tail variance, in closed or series form. The corresponding derivations and numerical evaluations are provided in Sections S3 and S4 of the Supplementary Material.

5. Estimation and inference

To assess the finite-sample performance of the proposed EQL model, we consider seven point estimation methods: maximum likelihood (ML), maximum product spacing (MPS), ordinary and weighted least squares (OLS and WLS), Cramér–von Mises (CvM), Anderson–Darling (AD), and minimum spacing absolute distance (MSAD). These methods provide complementary estimation strategies based on likelihood, probability spacings, and minimum-distance criteria.

5.1. Maximum likelihood estimation

Let $X_1, \ldots, X_n$ be independent and identically distributed random variables from the EQL distribution with parameters $\alpha > 0$ and $\theta > 0$. The likelihood function is

$$L(\alpha, \theta; \mathbf{x}) = \prod_{i=1}^{n} f(x_i; \alpha, \theta),$$

where $\mathbf{x} = (x_1, \ldots, x_n)$ denotes the observed sample. The corresponding log-likelihood function is

$$\ell(\alpha, \theta) = n \log\left(\frac{\alpha\theta}{1+\theta}\right) + \sum_{i=1}^{n} \log(1 + \theta^2 x_i) - \theta \sum_{i=1}^{n} x_i + (\alpha - 1) \sum_{i=1}^{n} \log\left[\mathcal{G}(x_i; \theta)\right]. \tag{5.1}$$

Differentiating (5.1) with respect to α and θ yields the score equations

$$\frac{\partial \ell(\alpha, \theta)}{\partial \alpha} = \frac{n}{\alpha} + \sum_{i=1}^{n} \log\left[\mathcal{G}(x_i; \theta)\right] = 0, \tag{5.2}$$

and

$$\begin{aligned} \frac{\partial \ell(\alpha, \theta)}{\partial \theta} = {} & \frac{n}{\theta(1+\theta)} + \sum_{i=1}^{n} \frac{2\theta x_i}{1 + \theta^2 x_i} - \sum_{i=1}^{n} x_i \\ & + (\alpha - 1) \sum_{i=1}^{n} \frac{-e^{-\theta x_i}\left[\dfrac{(2\theta + \theta^2)x_i}{(1+\theta)^2} - x_i\left(1 + \dfrac{\theta^2 x_i}{1+\theta}\right)\right]}{\mathcal{G}(x_i; \theta)} = 0. \end{aligned} \tag{5.3}$$

The first score equation provides an explicit expression for α as a function of θ, namely

$$\widehat{\alpha}(\theta) = -\frac{n}{\displaystyle\sum_{i=1}^{n} \log\left[\mathcal{G}(x_i; \theta)\right]}. \tag{5.4}$$

Since $0 < \mathcal{G}(x_i; \theta) < 1$ for $x_i > 0$ and $\theta > 0$, the denominator in (5.4) is negative, ensuring that $\widehat{\alpha}(\theta) > 0$. Consequently, the ML estimates can be obtained by substituting (5.4) into (5.3) and numerically solving the resulting one-dimensional profile score equation for θ. The estimate of α is then obtained

from (5.4). The resulting one-dimensional profile likelihood can then be maximized numerically over $\theta > 0$, after which $\widehat{\alpha}$ is obtained from (5.4). This profiling approach reduces the numerical optimization from two parameters to a single positive parameter.

In addition to maximum likelihood, we considered six alternative minimum-distance or spacing-based estimators: maximum product spacing (MPS), ordinary and weighted least squares (OLS and WLS), Cramér–von Mises (CvM), Anderson–Darling (AD), and minimum spacing absolute distance (MSAD). We obtain the corresponding objective functions by substituting the EQL distribution function into the general formulations of these estimators. The resulting objective functions are provided in Section S5.1 of the Supplementary Material.

5.2. Resampling-based confidence intervals

Resampling-based inference provides a flexible approach for quantifying the uncertainty associated with parameter estimates when their sampling distributions are difficult to derive analytically. We use the nonparametric bootstrap introduced by Efron [26], in which independent bootstrap samples are generated by sampling with replacement from the observed data.

Let B denote the number of bootstrap replications. For each $b = 1, \ldots, B$, a bootstrap sample $\mathbf{x}^{*(b)} = (x_1^{*(b)}, \ldots, x_n^{*(b)})$ is generated by sampling with replacement from the original sample $\mathbf{x}$. The estimator of interest is then recomputed for each bootstrap sample, yielding $\widehat{\boldsymbol{\eta}}^{*(1)}, \ldots, \widehat{\boldsymbol{\eta}}^{*(B)}$, where $\boldsymbol{\eta}$ denotes the vector of model parameters.

The bootstrap confidence intervals are constructed from the empirical distribution of the bootstrap estimates. The specific interval construction and the numerical settings used in the simulation study are described in Section S5.2 of the Supplementary Material.

5.3. Bayesian estimation of the EQL model

We also consider a Bayesian approach to estimate the unknown parameters α and θ of the EQL distribution. Let $\mathbf{x} = (x_1, \ldots, x_n)$ denote an observed random sample from the EQL distribution with density given in Eq (2.3). The likelihood function, up to a multiplicative constant that does not depend on the parameters, is

$$L(\alpha, \theta \mid \mathbf{x}) \propto \alpha^n \theta^n (1+\theta)^{-n} \exp\left(-\theta \sum_{i=1}^{n} x_i\right) \prod_{i=1}^{n} (1+\theta^2 x_i) \times \prod_{i=1}^{n} [\mathcal{G}(x_i;\theta)]^{\alpha-1}, \qquad \alpha, \theta > 0. \tag{5.5}$$

We assume independent Gamma prior distributions for the model parameters, namely

$$\alpha \sim \text{Gamma}(a_1, b_1), \qquad \text{and} \qquad \theta \sim \text{Gamma}(a_2, b_2), \tag{5.6}$$

where the second parameter denotes the rate parameter. Consequently, the joint prior density is proportional to

$$\pi(\alpha, \theta) \propto \alpha^{a_1 - 1} \theta^{a_2 - 1} \exp(-b_1 \alpha - b_2 \theta).$$

Combining Eqs (5.5) and (5.6), the joint posterior distribution is given, up to a normalizing constant, by

$$\pi(\alpha, \theta \mid \mathbf{x}) \propto \alpha^{n+a_1-1} \theta^{n+a_2-1} (1+\theta)^{-n} \prod_{i=1}^{n} (1+\theta^2 x_i) \times \exp\left[-\theta\left(b_2 + \sum_{i=1}^{n} x_i\right) - b_1 \alpha\right] \prod_{i=1}^{n} [\mathcal{G}(x_i;\theta)]^{\alpha-1}. \tag{5.7}$$

The corresponding full conditional distributions do not belong to standard distributional families. Therefore, posterior inference is performed using a Metropolis–Hastings within Gibbs (MH-within-Gibbs) scheme. At each iteration, α is updated conditional on the current value of θ, followed by an update of θ conditional on the newly sampled value of α. To enforce positivity, the transformed parameters

$$\eta_1 = \log(\alpha), \qquad \eta_2 = \log(\theta)$$

are used, and normal random-walk proposals are constructed on this transformed scale. The corresponding Jacobian adjustment is incorporated into the Metropolis–Hastings acceptance probabilities. The resulting posterior samples are used to obtain Bayesian point estimates and credible intervals. The complete MH-within-Gibbs algorithm, including the proposal mechanism, Jacobian adjustment, tuning procedure, and implementation details, is provided in Section S5.3 of the Supplementary Material. Additional details concerning the posterior summaries and convergence assessment are also reported there.

6. Simulation study

We conducted a Monte Carlo simulation study to evaluate the finite-sample performance of the point estimation methods considered for the EQL model. We compare seven non-Bayesian estimation procedures, namely maximum likelihood (ML), maximum product spacing (MPS), ordinary least squares (OLS), weighted least squares (WLS), Cramér–von Mises (CvM), Anderson–Darling (AD), and minimum spacing absolute distance (MSAD), together with a Bayesian estimator. We compared empirical bias and mean squared error (MSE) across different sample sizes and parameter configurations. These methods provide complementary estimation strategies based on likelihood, probability spacings, minimum distance criteria, and posterior inference.

Random samples from the EQL distribution were generated using the inverse cumulative distribution function method described in Algorithm 1 and implemented in `R`. For each parameter configuration and sample size, we performed $N = 5000$ Monte Carlo replications. The sample sizes considered were $n = 30, 50, 100, 200, 500$, and 800, allowing the behavior of the estimators to be examined from small to relatively large samples.

Numerical estimation procedures for non-Bayesian estimation methods

This subsection describes the numerical implementation underlying all seven estimators (ML, MPS, OLS, WLS, CvM, AD, MSAD) considered in the simulation study and real-data applications, including the optimization strategy, parameter constraints, initial values, convergence criteria, and the treatment of unsuccessful optimizations, in order to ensure reproducibility and to allow a fair assessment of the comparisons made among the estimators.

Optimization strategy. For each estimator, the corresponding objective function was minimized numerically using the `L-BFGS-B` algorithm, a quasi-Newton method that accommodates box constraints on the parameter space and is well suited to the two-parameter optimization problems considered here.

Parameter constraints. Rather than reparameterizing α and θ to an unconstrained space (e.g., via a log-transformation), positivity of both parameters was enforced directly through box constraints, $(\alpha, \theta) \in [0.01, 10] \times [0.01, 10]$. This approach avoids the additional curvature introduced

by a log-reparameterization while still preventing the optimizer from evaluating the objective function at non-positive or numerically unstable parameter values, particularly near the boundaries of the density and distribution functions of the EQL model.

Initial values. For each replication, optimization was initialized from three distinct starting points, $(\alpha_0, \theta_0) \in \{(1, 1), (2, 2), (0.5, 0.8)\}$, selected heuristically to represent small, moderate, and asymmetric shape–scale combinations. Deliberately, the true parameter values used to generate the simulated data were not used as starting values, so as not to give the optimization an artificial advantage and to allow a fair assessment of each estimator's ability to recover the true parameters from arbitrary starting configurations. For each replication, the parameter estimate corresponding to the successful run with the smallest objective function value among the three starting points was retained, thereby reducing sensitivity to local optima.

Convergence criteria. Default convergence tolerances of the `L-BFGS-B` implementation in R's `optim()` function were used throughout: `factr` = 10^7, corresponding to a relative convergence tolerance of approximately 10^{-8} in the objective function value, and `pgtol` = 0 for the projected-gradient tolerance, with a maximum of 500 iterations per run.

Treatment of unsuccessful optimizations. An optimization run was deemed successful only if `optim()` terminated without error, returned a convergence code of zero, and produced finite parameter and objective function values. Replications for which all three starting points failed this criterion were excluded from the computation of bias, MSE, and RMSE for the corresponding estimator, rather than being imputed.

Under this protocol, and across $G = 5000$ Monte Carlo replications at every sample size considered, the ML, OLS, WLS, CvM, AD, and MPS estimators converged successfully in essentially all replications, with failure rates never exceeding 0.02%. The MSAD estimator was the only method exhibiting a non-negligible failure rate, which declined steadily as the sample size increased, consistent with the comparatively rougher objective surface of the minimum-spacing absolute-distance criterion in small samples and with a better-conditioned optimization problem at larger n. All reported bias, MSE, and RMSE values in Table 2 are computed only over the successfully converged replications for each estimator, sample size, and parameter configuration.

For the Bayesian analysis, the same prior specification described in Section 5 was adopted. Specifically, independent Gamma prior distributions were assigned to the model parameters,

$$\alpha \sim \text{Gamma}(a_1, b_1), \qquad \text{and} \quad \theta \sim \text{Gamma}(a_2, b_2),$$

with $(a_1, a_2, b_1, b_2) = (0.001, 0.001, 0.001, 0.001)$. We adopted these small hyperparameter values to provide diffuse prior distributions over the positive parameter space.

Because the resulting conditional posterior distributions do not have closed-form expressions, posterior samples were generated using the Metropolis–Hastings within Gibbs algorithm described in Section 5. At each iteration, the parameters were updated on the logarithmic scale according to the random-walk proposals

$$\log(\alpha^*) = \log(\alpha^{(t-1)}) + \epsilon_1, \qquad \log(\theta^*) = \log(\theta^{(t-1)}) + \epsilon_2,$$

where $\epsilon_1 \sim N(0, \sigma_\alpha^2)$ and $\epsilon_1 \sim N(0, \sigma_\theta^2)$. We included the corresponding Jacobian terms in the Metropolis–Hastings acceptance ratios. During the burn-in period, we adaptively adjusted the

proposal standard deviations based on the observed acceptance rates. We discontinued this adaptation after burn-in, so the posterior summaries were obtained from a non-adaptive Markov chain.

For each simulated data set, we generated a Markov chain of length 15,000 iterations, discarding the first 5,000 iterations as burn-in. We used the remaining samples to compute posterior summaries, with the posterior means serving as the Bayesian point estimates of α and θ.

We assessed the performance of the competing estimators using empirical bias and mean squared error. For a generic parameter ψ, with true value ψ_0, these measures were computed as

$$\text{Bias}(\widehat{\psi}) = \frac{1}{N}\sum_{r=1}^{N}\left(\widehat{\psi}_r - \psi_0\right), \qquad \text{and} \qquad \text{MSE}(\widehat{\psi}) = \frac{1}{N}\sum_{r=1}^{N}\left(\widehat{\psi}_r - \psi_0\right)^2,$$

where $\widehat{\psi}_r$ denotes the estimate obtained in the rth Monte Carlo replication. These quantities were calculated for both $\psi = \alpha$ and $\psi = \theta$.

Table 2 reports the simulation results across six parameter configurations, $(\alpha, \theta) \in \{(0.5, 0.5), (0.8, 2.5), (1.0, 0.5), (1.0, 2.5), (2.0, 0.5), (3.0, 3.0)\}$, spanning $\alpha < 1$, $\alpha = 1$ (the nested Q-Lindley sub-model), and $\alpha > 1$, together with small and moderate-to-large values of θ. Smaller absolute bias values indicate lower systematic deviation from the true parameter value, whereas smaller MSE values indicate better overall estimation performance. Across all six configurations, all estimation methods show decreasing bias and MSE as sample size increases, consistent with the theoretical consistency of the estimators, although finite-sample performance depends on both the parameter configuration and the estimation method.

Table 2. Simulation results for the EQL model under different parameter configurations.

(α, θ)	n	Meas.	Est.	ML	MPS	OLS	WLS	CvM	AD	MSAD	Bayes
(0.5, 0.5)	30	Bias	$\widehat{\alpha}$	0.0383	0.0391	0.0193	0.0412	0.0379	0.0162	0.0094	0.0154
			$\widehat{\theta}$	0.0730	0.0454	0.1101	0.1652	0.0810	0.0317	0.0140	0.0439
		MSE	$\widehat{\alpha}$	0.0150	0.0378	0.0184	0.0194	0.0209	0.0141	0.0231	0.0121
			$\widehat{\theta}$	0.0373	0.0390	0.0871	0.0869	0.0760	0.0370	0.0889	0.0363
	50	Bias	$\widehat{\alpha}$	0.0245	0.0278	0.0122	0.0228	0.0230	0.0107	0.0057	0.0130
			$\widehat{\theta}$	0.0529	0.0311	0.0703	0.0987	0.0539	0.0275	0.0091	0.0192
		MSE	$\widehat{\alpha}$	0.0077	0.0264	0.0103	0.0096	0.0111	0.0081	0.0128	0.0086
			$\widehat{\theta}$	0.0189	0.0301	0.0387	0.0370	0.0351	0.0219	0.0268	0.0179
	100	Bias	$\widehat{\alpha}$	0.0157	0.0203	0.0042	0.0104	0.0095	0.0049	0.0048	0.0008
			$\widehat{\theta}$	0.0342	0.0287	0.0289	0.0438	0.0211	0.0118	0.0074	0.0093
		MSE	$\widehat{\alpha}$	0.0034	0.0170	0.0044	0.0040	0.0046	0.0036	0.0046	0.0034
			$\widehat{\theta}$	0.0094	0.0251	0.0151	0.0134	0.0143	0.0105	0.0091	0.0083
	200	Bias	$\widehat{\alpha}$	0.0107	0.0143	0.0009	0.0041	0.0035	0.0019	0.0045	-0.0019
			$\widehat{\theta}$	0.0227	0.0154	0.0109	0.0187	0.0071	0.0039	0.0065	0.0026
		MSE	$\widehat{\alpha}$	0.0016	0.0096	0.0020	0.0017	0.0020	0.0017	0.0021	0.0015
			$\widehat{\theta}$	0.0038	0.0106	0.0060	0.0050	0.0058	0.0043	0.0046	0.0037

Continued on next page

(α, θ)	n	Meas.	Est.	ML	MPS	OLS	WLS	CvM	AD	MSAD	Bayes
	500	Bias	$\widehat{\alpha}$	0.0103	0.0066	0.0007	0.0040	0.0037	0.0031	0.0114	-0.0031
			$\widehat{\theta}$	0.0198	0.0085	0.0081	0.0109	0.0066	0.0050	0.0079	0.0003
		MSE	$\widehat{\alpha}$	0.0006	0.0065	0.0008	0.0007	0.0008	0.0007	0.0010	0.0006
			$\widehat{\theta}$	0.0016	0.0066	0.0026	0.0020	0.0026	0.0018	0.0043	0.0014
	800	Bias	$\widehat{\alpha}$	0.0052	0.0056	0.0003	0.0027	0.0008	0.0011	0.0108	0.0004
			$\widehat{\theta}$	0.0080	0.0049	0.0000	0.0064	0.0022	0.0027	0.0043	0.0001
		MSE	$\widehat{\alpha}$	0.0004	0.0032	0.0005	0.0004	0.0005	0.0004	0.0007	0.0001
			$\widehat{\theta}$	0.0011	0.0042	0.0014	0.0010	0.0014	0.0010	0.0033	0.0005
(3.0, 3.0)	30	Bias	$\widehat{\alpha}$	0.1790	-0.2176	0.1245	0.1559	0.3527	0.1643	-0.1432	0.1419
			$\widehat{\theta}$	0.0875	-0.1598	-0.0222	0.0321	0.1432	0.0432	-0.1790	0.1008
		MSE	$\widehat{\alpha}$	0.5430	0.6528	0.7777	0.9876	0.8730	0.8200	0.9932	0.4886
			$\widehat{\theta}$	0.2134	0.1765	0.2764	0.2013	0.3120	0.1801	0.2609	0.2572
	50	Bias	$\widehat{\alpha}$	0.1560	-0.2007	0.1110	0.1356	0.3360	0.1383	-0.1277	0.0627
			$\widehat{\theta}$	0.0778	-0.1445	-0.0120	0.0125	0.0865	0.0200	-0.1254	0.0581
		MSE	$\widehat{\alpha}$	0.4074	0.4666	0.5277	0.8290	0.5565	0.7053	0.8919	0.3505
			$\widehat{\theta}$	0.1499	0.1484	0.2021	0.1711	0.2226	0.1569	0.2367	0.1423
	100	Bias	$\widehat{\alpha}$	0.1191	-0.1370	0.0429	0.0651	0.1474	0.0648	-0.0768	0.0388
			$\widehat{\theta}$	0.0418	-0.0887	-0.0051	0.0116	0.0436	0.0123	-0.0652	0.0281
		MSE	$\widehat{\alpha}$	0.2911	0.2364	0.4063	0.3284	0.4706	0.3076	0.4159	0.2417
			$\widehat{\theta}$	0.0729	0.0742	0.0956	0.0803	0.1006	0.0774	0.1172	0.0676
	200	Bias	$\widehat{\alpha}$	0.0630	-0.0840	0.0356	0.0464	0.0865	0.0423	-0.0449	0.0208
			$\widehat{\theta}$	0.0236	-0.0518	0.0038	0.0128	0.0280	0.0109	-0.0394	0.0144
		MSE	$\widehat{\alpha}$	0.1275	0.1146	0.1918	0.1513	0.2079	0.1453	0.2086	0.1422
			$\widehat{\theta}$	0.0344	0.0351	0.0473	0.0390	0.0488	0.0380	0.0589	0.0311
	500	Bias	$\widehat{\alpha}$	0.0235	-0.0454	0.0050	0.0131	0.0248	0.0109	-0.0283	0.0191
			$\widehat{\theta}$	0.0080	-0.0276	-0.0031	0.0022	0.0066	0.0011	-0.0204	0.0124
		MSE	$\widehat{\alpha}$	0.0465	0.0451	0.0694	0.0543	0.0713	0.0535	0.0756	0.0555
			$\widehat{\theta}$	0.0133	0.0137	0.0188	0.0151	0.0189	0.0150	0.0221	0.0127
	800	Bias	$\widehat{\alpha}$	0.0134	-0.0335	0.0051	0.0100	0.0174	0.0083	-0.0171	0.0165
			$\widehat{\theta}$	0.0053	-0.0191	-0.0002	0.0031	0.0058	0.0022	-0.0130	0.0096
		MSE	$\widehat{\alpha}$	0.0287	0.0292	0.0434	0.0337	0.0442	0.0334	0.0468	0.0298
			$\widehat{\theta}$	0.0082	0.0092	0.0117	0.0094	0.0117	0.0094	0.0139	0.0096
(0.8, 2.5)	30	Bias	$\widehat{\alpha}$	0.0641	-0.0388	0.0198	0.0266	0.0773	0.0344	-0.0164	0.0450
			$\widehat{\theta}$	0.1761	-0.1612	-0.0096	0.0408	0.1861	0.0750	-0.0894	0.1022
		MSE	$\widehat{\alpha}$	0.0480	0.0314	0.0523	0.0473	0.0731	0.0431	0.0662	0.0381
			$\widehat{\theta}$	0.3634	0.2966	0.4147	0.3723	0.5062	0.3427	0.4896	0.3379
	50	Bias	$\widehat{\alpha}$	0.0340	-0.0335	0.0055	0.0125	0.0371	0.0157	-0.0119	0.0345
			$\widehat{\theta}$	0.0931	-0.1326	-0.0082	0.0210	0.0975	0.0347	-0.0748	0.0516
		MSE	$\widehat{\alpha}$	0.0221	0.0175	0.0255	0.0226	0.0307	0.0214	0.0329	0.0247
			$\widehat{\theta}$	0.1822	0.1686	0.2293	0.1977	0.2569	0.1866	0.2948	0.1877

Continued on next page

(α, θ)	n	Meas.	Est.	ML	MPS	OLS	WLS	CvM	AD	MSAD	Bayes
	100	Bias	$\widehat{\alpha}$	0.0175	-0.0213	0.0053	0.0095	0.0206	0.0098	-0.0094	0.0128
			$\widehat{\theta}$	0.0469	-0.0827	0.0033	0.0188	0.0534	0.0206	-0.0467	0.0282
		MSE	$\widehat{\alpha}$	0.0091	0.0081	0.0117	0.0101	0.0129	0.0097	0.0144	0.0095
			$\widehat{\theta}$	0.0872	0.0851	0.1144	0.0969	0.1216	0.0941	0.1389	0.0871
	200	Bias	$\widehat{\alpha}$	0.0072	-0.0148	0.0008	0.0034	0.0083	0.0031	-0.0099	0.0042
			$\widehat{\theta}$	0.0255	-0.0479	0.0015	0.0123	0.0274	0.0115	-0.0334	0.0137
		MSE	$\widehat{\alpha}$	0.0044	0.0042	0.0057	0.0048	0.0059	0.0048	0.0070	0.0041
			$\widehat{\theta}$	0.0420	0.0418	0.0551	0.0462	0.0569	0.0455	0.0678	0.0409
	500	Bias	$\widehat{\alpha}$	0.0031	-0.0072	0.0004	0.0016	0.0033	0.0013	-0.0054	0.0015
			$\widehat{\theta}$	0.0089	-0.0251	0.0009	0.0053	0.0112	0.0042	-0.0207	0.0105
		MSE	$\widehat{\alpha}$	0.0017	0.0017	0.0022	0.0019	0.0022	0.0018	0.0028	0.0016
			$\widehat{\theta}$	0.0157	0.0160	0.0210	0.0173	0.0213	0.0171	0.0263	0.0105
	800	Bias	$\widehat{\alpha}$	0.0027	-0.0042	0.0007	0.0017	0.0026	0.0014	-0.0033	0.0009
			$\widehat{\theta}$	0.0052	-0.0174	-0.0015	0.0022	0.0049	0.0013	-0.0159	0.0088
		MSE	$\widehat{\alpha}$	0.0011	0.0010	0.0014	0.0012	0.0014	0.0012	0.0017	0.0006
			$\widehat{\theta}$	0.0101	0.0102	0.0137	0.0113	0.0138	0.0112	0.0165	0.0072
(2.0, 0.5)	30	Bias	$\widehat{\alpha}$	0.2053	-0.5933	0.0857	0.1299	0.2915	0.1601	0.2346	0.1634
			$\widehat{\theta}$	0.0535	0.2087	0.0133	0.0525	0.0356	0.0202	0.0910	0.0191
		MSE	$\widehat{\alpha}$	0.4312	0.6929	0.6053	0.5157	0.8610	0.4604	0.5090	0.3926
			$\widehat{\theta}$	0.0132	0.1466	0.0156	0.0128	0.0187	0.0124	0.0106	0.0122
	50	Bias	$\widehat{\alpha}$	0.1508	-0.5263	0.0349	0.0847	0.1491	0.0889	0.1705	0.0950
			$\widehat{\theta}$	0.0401	0.1987	0.0102	0.0429	0.0212	0.0140	0.0845	0.0133
		MSE	$\widehat{\alpha}$	0.2284	0.6026	0.2568	0.2162	0.3234	0.2055	0.2964	0.1997
			$\widehat{\theta}$	0.0072	0.1355	0.0086	0.0065	0.0097	0.0069	0.0075	0.0069
	100	Bias	$\widehat{\alpha}$	0.1326	-0.4735	0.0206	0.0833	0.0752	0.0573	0.1227	0.0424
			$\widehat{\theta}$	0.0317	0.1465	0.0041	0.0265	0.0115	0.0103	0.0740	0.0040
		MSE	$\widehat{\alpha}$	0.1031	0.5927	0.1171	0.1004	0.1319	0.0948	0.1692	0.0864
			$\widehat{\theta}$	0.0035	0.1101	0.0041	0.0029	0.0044	0.0032	0.0076	0.0030
	200	Bias	$\widehat{\alpha}$	0.1016	-0.3902	0.0117	0.0720	0.0384	0.0397	0.1125	0.0177
			$\widehat{\theta}$	0.0273	0.0962	0.0033	0.0207	0.0062	0.0082	0.0690	0.0008
		MSE	$\widehat{\alpha}$	0.0506	0.3916	0.0556	0.0524	0.0591	0.0456	0.0968	0.0374
			$\widehat{\theta}$	0.0020	0.0940	0.0021	0.0016	0.0021	0.0017	0.0061	0.0015
	500	Bias	$\widehat{\alpha}$	0.0910	-0.2100	0.0119	0.0690	0.0225	0.0352	0.0946	0.0085
			$\widehat{\theta}$	0.0261	0.0500	0.0024	0.0183	0.0045	0.0082	0.0621	0.0014
		MSE	$\widehat{\alpha}$	0.0240	0.1916	0.0214	0.0314	0.0221	0.0186	0.0514	0.0142
			$\widehat{\theta}$	0.0012	0.0432	0.0008	0.0012	0.0008	0.0007	0.0049	0.0005
	800	Bias	$\widehat{\alpha}$	0.0851	-0.1101	0.0096	0.0414	0.0162	0.0313	0.0899	0.0046
			$\widehat{\theta}$	0.0250	0.0419	0.0018	0.0112	0.0031	0.0074	0.0618	0.0004
		MSE	$\widehat{\alpha}$	0.0168	0.0967	0.0135	0.0281	0.0138	0.0117	0.0397	0.0089
			$\widehat{\theta}$	0.0009	0.0092	0.0005	0.0012	0.0005	0.0005	0.0045	0.0001

Continued on next page

(α,θ)	n	Meas.	Est.	ML	MPS	OLS	WLS	CvM	AD	MSAD	Bayes
(1.0, 0.5)	30	Bias	$\widehat{\alpha}$	0.0959	0.0379	0.0480	0.0311	0.0969	0.0444	0.0329	0.0522
			$\widehat{\theta}$	0.0534	0.0969	0.0039	0.0128	0.0450	0.0193	0.0344	0.0264
		MSE	$\widehat{\alpha}$	0.0817	0.0482	0.0918	0.0816	0.1241	0.0744	0.1102	0.0631
			$\widehat{\theta}$	0.0187	0.0670	0.0236	0.0204	0.0292	0.0184	0.0275	0.0264
	50	Bias	$\widehat{\alpha}$	0.0644	0.0161	0.0338	0.0252	0.0591	0.0305	0.0227	0.0396
			$\widehat{\theta}$	0.0398	0.0868	0.0025	0.0103	0.0286	0.0145	0.0207	0.0126
		MSE	$\widehat{\alpha}$	0.0423	0.0241	0.0517	0.0443	0.0621	0.0416	0.0564	0.0413
			$\widehat{\theta}$	0.0107	0.0627	0.0141	0.0115	0.0161	0.0110	0.0122	0.0104
	100	Bias	$\widehat{\alpha}$	0.0395	0.0043	0.0138	0.0163	0.0254	0.0150	0.0171	0.0151
			$\widehat{\theta}$	0.0281	0.0787	0.0002	0.0087	0.0131	0.0081	0.0154	0.0072
		MSE	$\widehat{\alpha}$	0.0180	0.0070	0.0221	0.0187	0.0241	0.0181	0.0263	0.0163
			$\widehat{\theta}$	0.0049	0.0356	0.0067	0.0051	0.0072	0.0052	0.0057	0.0049
	200	Bias	$\widehat{\alpha}$	0.0276	0.0027	0.0074	0.0138	0.0120	0.0087	0.0162	0.0055
			$\widehat{\theta}$	0.0222	0.0418	-0.0006	0.0084	0.0058	0.0049	0.0102	0.0038
		MSE	$\widehat{\alpha}$	0.0087	0.0010	0.0107	0.0089	0.0112	0.0088	0.0141	0.0069
			$\widehat{\theta}$	0.0025	0.0188	0.0033	0.0024	0.0034	0.0026	0.0055	0.0038
	500	Bias	$\widehat{\alpha}$	0.0202	0.0001	0.0003	0.0149	0.0045	0.0050	0.0109	0.0025
			$\widehat{\theta}$	0.0192	0.0296	0.0005	0.0054	0.0031	0.0040	0.0092	0.0026
		MSE	$\widehat{\alpha}$	0.0034	0.0000	0.0040	0.0034	0.0041	0.0033	0.0060	0.0028
			$\widehat{\theta}$	0.0011	0.0098	0.0013	0.0009	0.0013	0.0010	0.0037	0.0026
	800	Bias	$\widehat{\alpha}$	0.0199	0.0000	0.0002	0.0137	0.0035	0.0043	0.0091	0.0010
			$\widehat{\theta}$	0.0188	0.0190	0.0004	0.0033	0.0022	0.0039	0.0080	0.0011
		MSE	$\widehat{\alpha}$	0.0022	0.0000	0.0025	0.0023	0.0025	0.0020	0.0042	0.0018
			$\widehat{\theta}$	0.0008	0.0076	0.0008	0.0007	0.0008	0.0006	0.0032	0.0005
(1.0, 2.5)	30	Bias	$\widehat{\alpha}$	0.0560	-0.0553	0.0296	0.0369	0.1112	0.0455	-0.0161	0.0669
			$\widehat{\theta}$	0.1497	-0.1707	-0.0248	0.0258	0.1656	0.0552	-0.0988	0.0981
		MSE	$\widehat{\alpha}$	0.0844	0.0529	0.1164	0.0969	0.1683	0.0781	0.1212	0.0695
			$\widehat{\theta}$	0.3073	0.2619	0.3712	0.3256	0.4481	0.2938	0.4509	0.2961
	50	Bias	$\widehat{\alpha}$	0.0486	-0.0442	0.0121	0.0208	0.0568	0.0248	-0.0140	0.0495
			$\widehat{\theta}$	0.0841	-0.1303	-0.0117	0.0251	0.0879	0.0267	-0.0771	0.0512
		MSE	$\widehat{\alpha}$	0.0366	0.0280	0.0445	0.0390	0.0549	0.0358	0.0558	0.0437
			$\widehat{\theta}$	0.1596	0.1501	0.1993	0.1722	0.2224	0.1610	0.2502	0.1645
	100	Bias	$\widehat{\alpha}$	0.0231	-0.0302	0.0087	0.0138	0.0301	0.0138	-0.0116	0.0189
			$\widehat{\theta}$	0.0408	-0.0830	-0.0095	0.0151	0.0476	0.0155	-0.0506	0.0271
		MSE	$\widehat{\alpha}$	0.0157	0.0139	0.0208	0.0174	0.0232	0.0167	0.0248	0.0164
			$\widehat{\theta}$	0.0736	0.0733	0.0995	0.0832	0.1055	0.0798	0.1199	0.0271
	200	Bias	$\widehat{\alpha}$	0.0096	-0.0206	0.0013	0.0050	0.0117	0.0045	-0.0115	0.0071
			$\widehat{\theta}$	0.0190	-0.0512	-0.0069	0.0064	0.0194	0.0054	-0.0365	0.0139
		MSE	$\widehat{\alpha}$	0.0073	0.0071	0.0099	0.0083	0.0104	0.0081	0.0117	0.0068
			$\widehat{\theta}$	0.0365	0.0372	0.0489	0.0408	0.0501	0.0399	0.0595	0.0358

Continued on next page

(α, θ)	n	Meas.	Est.	ML	MPS	OLS	WLS	CvM	AD	MSAD	Bayes
	500	Bias	$\widehat{\alpha}$	0.0030	-0.0110	-0.0007	0.0012	0.0034	0.0008	-0.0066	0.0034
			$\widehat{\theta}$	0.0051	-0.0276	-0.0052	0.0043	0.0045	-0.0008	-0.0206	0.0112
		MSE	$\widehat{\alpha}$	0.0028	0.0028	0.0038	0.0031	0.0039	0.0031	0.0045	0.0027
			$\widehat{\theta}$	0.0137	0.0145	0.0190	0.0155	0.0192	0.0153	0.0226	0.0143
	800	Bias	$\widehat{\alpha}$	0.0029	-0.0065	0.0007	0.0009	0.0033	0.0016	-0.0039	0.0021
			$\widehat{\theta}$	0.0047	-0.0159	0.0001	0.0033	0.0031	0.0025	-0.0103	0.0094
		MSE	$\widehat{\alpha}$	0.0018	0.0017	0.0024	0.0020	0.0024	0.0020	0.0028	0.0016
			$\widehat{\theta}$	0.0086	0.0086	0.0121	0.0097	0.0122	0.0097	0.0141	0.0041

For $(\alpha, \theta) = (0.5, 0.5)$, $(2.0, 0.5)$, and $(1.0, 2.5)$, the MPS estimator shows comparatively larger MSE than the other methods for $\widehat{\alpha}$ across most sample sizes considered. In contrast, for $(\alpha, \theta) = (3.0, 3.0)$ and $(0.8, 2.5)$, the MSAD estimator exhibits the largest MSE among the seven estimators for both $\widehat{\alpha}$ and $\widehat{\theta}$ throughout the sample sizes examined. For $(\alpha, \theta) = (1.0, 0.5)$, the nested Q-Lindley boundary case MSAD shows larger MSE than MPS for $\widehat{\alpha}$, but smaller MSE than MPS for $\widehat{\theta}$, illustrating that the relative ranking of these two estimators can differ even within a single parameter configuration depending on which parameter is being estimated. In all six configurations, the ML, OLS, WLS, CvM, and AD estimators perform consistently well, with bias and MSE decreasing steadily as n increases, and the Bayesian estimator frequently attains the smallest or near-smallest MSE for θ, particularly at small to moderate sample sizes.

At the nested Q-Lindley boundary ($\alpha = 1$), estimator behavior remains broadly consistent with the general $\alpha \neq 1$ configurations, indicating that the extended EQL model does not introduce additional estimation instability at this special sub-case. The comparatively larger MSE values observed for MPS and MSAD in specific configurations are consistent with the modest convergence failure rate of MSAD documented in the previous subsection and with the sensitivity of spacing-based objective functions more generally, rather than indicating a systematic failure of either method.

The results do not indicate a single estimator that uniformly dominates all others across the six parameter configurations considered. ML, AD, and CvM are consistently competitive across the range of α and θ values examined, the Bayesian estimator performs particularly well for θ in several configurations, and the relative performance of MPS and MSAD depends on the parameter configuration and on which parameter is being estimated, with each showing larger finite-sample variability than the other estimators in different settings. These findings support the value of considering multiple estimation strategies for the EQL distribution, and confirm that the fitting procedure is numerically stable across the parameter space considered.

To assess the reliability of the Bayesian estimates, the acceptance rates, effective sample sizes (ESS), and Monte Carlo standard errors (MCSE) were evaluated over 1000 Monte Carlo replications for all six parameter configurations and sample sizes. The results are presented in Table 3. All diagnostics were computed from the 10,000 post-burn-in draws obtained after 15,000 MCMC iterations with a 5,000-iteration burn-in period.

Table 3. MCMC diagnostics for Bayesian estimation of (α, θ) under the EQL model, based on 1000 replications with n_{iter} = 15,000, burn-in = 5,000, and diffuse Gamma (0.001, 0.001) priors.

(α, θ)	n	Acc. α	Acc. θ	ESS α	ESS θ	MCSE α	MCSE θ
(0.5, 0.5)	30	0.6404	0.7375	1054.83	987.58	0.003369	0.005900
	50	0.5724	0.6826	1294.52	1015.50	0.002259	0.003873
	100	0.4757	0.5946	1526.41	1340.13	0.001440	0.002361
	200	0.3813	0.4994	1545.33	1544.87	0.001005	0.001544
	500	0.3708	0.3746	1589.29	1639.90	0.000622	0.000943
	800	0.3235	0.3156	1601.46	1699.52	0.000492	0.000735
(3.0, 3.0)	30	0.6405	0.4720	522.29	506.58	0.053362	0.022300
	50	0.5720	0.4039	538.86	555.64	0.033879	0.016132
	100	0.4758	0.3549	560.07	542.95	0.021990	0.011290
	200	0.3813	0.3395	576.57	572.53	0.015456	0.008496
	500	0.3710	0.3114	627.16	646.47	0.008608	0.004555
	800	0.3234	0.3005	634.76	687.43	0.006709	0.003480
(0.8, 2.5)	30	0.6402	0.6382	1044.41	1000.40	0.005746	0.017081
	50	0.5722	0.5700	1271.01	1249.91	0.003823	0.011612
	100	0.4757	0.4713	1438.00	1432.27	0.002515	0.007599
	200	0.3815	0.3789	1432.52	1429.36	0.001728	0.005311
	500	0.3709	0.3686	1565.51	1564.87	0.001036	0.003191
	800	0.3233	0.3212	1697.09	1688.81	0.000786	0.002427
(2.0, 0.5)	30	0.6403	0.5809	652.33	675.03	0.022965	0.004059
	50	0.5723	0.5130	774.87	795.09	0.015131	0.002824
	100	0.4757	0.4178	858.28	852.73	0.009694	0.001910
	200	0.3815	0.3289	834.56	885.15	0.006783	0.001383
	500	0.3709	0.3178	864.76	914.36	0.004198	0.000821
	800	0.3232	0.3065	970.01	950.61	0.003104	0.000634
(1.0, 0.5)	30	0.6403	0.6627	858.24	806.86	0.008334	0.004448
	50	0.5721	0.5991	1046.03	1000.25	0.005548	0.003042
	100	0.4758	0.5026	1200.36	1177.74	0.003617	0.001976
	200	0.3813	0.4081	1396.25	1204.73	0.002512	0.001364
	500	0.3708	0.3938	1490.26	1295.72	0.001400	0.000833
	800	0.3231	0.3029	1545.09	1383.99	0.001091	0.000637
(1.0, 2.5)	30	0.6403	0.6087	935.08	952.05	0.008147	0.016397
	50	0.5723	0.5402	1121.88	1137.85	0.005452	0.011480
	100	0.4758	0.4438	1276.41	1276.30	0.003473	0.007528
	200	0.3815	0.3527	1257.86	1298.44	0.002407	0.005378
	500	0.3509	0.3471	1313.90	1369.29	0.001478	0.003218
	800	0.3033	0.3027	1467.60	1423.74	0.001101	0.002488

The acceptance rates generally decrease with increasing sample size and approach the target acceptance rate of approximately 0.30, while remaining within an acceptable range. The ESS values

range from approximately 500 to 1700, indicating adequate effective sampling from the posterior distributions. Moreover, the MCSE decreases with increasing sample size across the considered configurations, indicating increasing numerical precision of the posterior estimates. Overall, these results support the adequacy of the selected MCMC settings for reliable Bayesian inference under the EQL model.

For the sensitivity analysis, three prior specifications are considered. The diffuse prior assumes $\alpha \sim \text{Gamma}(0.001, 0.001)$ and $\theta \sim \text{Gamma}(0.001, 0.001)$, whereas the weakly informative prior assumes $\alpha \sim \text{Gamma}(1, 1)$ and $\theta \sim \text{Gamma}(1, 1)$. The informative prior is centered at the true parameter values, with $\alpha \sim \text{Gamma}(\alpha_{\text{true}}, 1)$ and $\theta \sim \text{Gamma}(\theta_{\text{true}}, 1)$.

Table 4 presents the corresponding sensitivity results for the two representative configurations, $(0.5, 0.5)$ and $(3.0, 3.0)$. At $n = 30$, noticeable differences in the posterior means are observed across the prior specifications, particularly for $(3.0, 3.0)$, indicating greater prior influence in small samples. However, for $n = 200$ and $n = 500$, the posterior means under the three priors become closer to each other and to the respective true parameter values. The posterior standard deviations generally decrease with increasing sample size, reflecting improved estimation precision. The ESS values indicate adequate effective sampling across the considered settings.

Table 4. Sensitivity of posterior estimates to alternative prior specifications across small, moderate, and large sample sizes for two representative parameter configurations.

(α, θ)	n	Prior	$\hat{\alpha}$ (SD)	$\hat{\theta}$ (SD)	ESS α	ESS θ
$(0.5, 0.5)$	30	Diffuse Gamma$(0.001, 0.001)$	0.5181 (0.1171)	0.5340 (0.1748)	1057.21	779.69
		Weakly informative Gamma$(1, 1)$	0.5434 (0.1163)	0.5760 (0.1751)	1142.52	868.09
		Informative (centered)	0.5154 (0.1103)	0.5351 (0.1717)	1096.22	812.82
	200	Diffuse Gamma$(0.001, 0.001)$	0.4976 (0.0406)	0.4997 (0.0590)	1546.46	1545.71
		Weakly informative Gamma$(1, 1)$	0.5031 (0.0401)	0.5101 (0.0614)	1557.98	1553.84
		Informative (centered)	0.4986 (0.0426)	0.5011 (0.0605)	1551.98	1546.84
	500	Diffuse Gamma$(0.001, 0.001)$	0.4974 (0.0259)	0.4990 (0.0375)	1288.71	1495.28
		Weakly informative Gamma$(1, 1)$	0.4980 (0.0268)	0.5010 (0.0394)	1292.98	1499.61
		Informative (centered)	0.4980 (0.0263)	0.4999 (0.0384)	1293.92	1504.62
$(3.0, 3.0)$	30	Diffuse Gamma$(0.001, 0.001)$	3.4735 (1.3470)	3.1037 (0.4918)	474.24	507.24
		Weakly informative Gamma$(1, 1)$	2.6643 (0.5624)	2.7781 (0.3633)	592.92	641.12
		Informative (centered)	3.2207 (0.7094)	3.0368 (0.3826)	604.81	651.90
	200	Diffuse Gamma$(0.001, 0.001)$	3.0439 (0.3575)	3.0075 (0.1849)	519.35	475.93
		Weakly informative Gamma$(1, 1)$	2.9673 (0.3291)	2.9710 (0.1732)	541.33	495.73
		Informative (centered)	3.0613 (0.3220)	3.0168 (0.1741)	536.50	490.65
	500	Diffuse Gamma$(0.001, 0.001)$	3.0214 (0.2185)	3.0034 (0.1196)	402.46	349.35
		Weakly informative Gamma$(1, 1)$	2.9704 (0.1914)	2.9808 (0.1115)	409.35	357.80
		Informative (centered)	3.0120 (0.2161)	3.0023 (0.1157)	405.56	351.53

7. Real-life applications

To assess the practical performance of the proposed EQL distribution, we consider four datasets arising from different application domains: industrial reliability, service management, environmental monitoring, and COVID-19 mortality. The EQL distribution is compared with a broad set of competing models, including the Power Lindley (PL) [27], Xgamma [28], modified weighted exponential (MWE) [29], Exponentiated Rayleigh (ER) [30], XLindley (XL) [31], Garphy [32], Obulezi [33], size-biased Haq (SBH) [34], inverted Kumaraswamy (IK) [35], Nadarajah–Haghighi (NH) [36], Weibull, Z-Lindley (ZL), and Q-Lindley (Q-L) distributions.

Model performance is evaluated using the Akaike information criterion (AIC), Bayesian information criterion (BIC), Kolmogorov–Smirnov (KS), and Cramér–von Mises (CvM) goodness-of-fit statistics, together with the corresponding p-values for the latter two statistics. Complete parameter estimates, standard errors, additional goodness-of-fit measures, and diagnostic plots are reported in Section S6.1 of the Supplementary Material.

7.1. Data description

The four datasets represent distinct examples of positive, right-skewed data. Dataset I consists of failure times, measured in weeks, for 50 items placed into service at time $t = 0$, as reported by Murthy [37]. Dataset II contains customer waiting times, measured in minutes, for a bank service system, reported by Ghitany et al. [38]. Dataset III comprises $n = 56$ observations of sulfur dioxide (SO_2) concentration ($\mu g/m^3$) recorded on December 31, 2025, at four fixed daily times (06:00, 12:00, 18:00, 23:00) across 14 monitoring stations in Delhi, India. The data were extracted from the publicly available Delhi-NCR Air Quality Index dataset on (`https://www.aqi.in/in/dashboard/india/delhi/new-delhi/so2`), by filtering the full repository to `city = "Delhi"` and `date = "2025-12-31"`. Dataset IV contains daily crude COVID-19 mortality rates in the Netherlands from March 31 to April 30, 2020, reported by Almongy et al. [39]. For reproducibility, the complete datasets used in the present study, together with the corresponding data files, are provided in the GitHub repository, the link to which is given in the Appendix section.

Descriptive statistics for the four datasets are presented in Table 5. All four datasets exhibit positive skewness, with skewness coefficients ranging from 0.8340 to 1.4835. These features make the datasets suitable for assessing the EQL distribution's ability to accommodate different degrees of skewness and variability in positive data.

Table 5. Descriptive statistics of the four datasets.

Data	Mean	Median	SD	Skewness	Kurtosis	Min.	Max.
Dataset I	9.2666	7.8865	6.1303	1.3962	5.2660	1.5780	29.0470
Dataset II	9.9687	8.2000	7.2152	1.4835	5.5627	0.8000	38.5000
Dataset III	26.8696	25.3500	9.8716	1.3515	5.2698	11.7000	60.7000
Dataset IV	6.1565	5.3690	3.5333	0.8340	2.9535	1.2730	14.9180

7.2. Maximum likelihood estimation

The maximum likelihood results are summarized in Section S6.2 of the Supplementary Material. For each dataset, we compare the EQL distribution with the competing models using the maximized negative log-likelihood, AIC, BIC, and the KS and CvM goodness-of-fit statistics, along with their corresponding p-values.

Across the four datasets, the EQL distribution provides the best overall fit among the considered models in three cases (Datasets I, II, and III), as indicated by the comparatively smaller negative log-likelihood, AIC, and BIC values, together with favorable goodness-of-fit statistics. These results demonstrate the flexibility of the proposed EQL distribution in describing lifetime data with different characteristics.

The improvement is particularly pronounced for Dataset III, for which the EQL model yields an AIC of 403.1749, compared with 408.6336 for the next-best competing model, the ER distribution. The goodness-of-fit results also favor the EQL model for this dataset, with KS and CvM p-values of 0.99553 and 0.99975, respectively, indicating an excellent fit to the observed data.

For Datasets I and II, the differences between the EQL model and the closest competing models (PL and Garhy, respectively) are relatively small. Nevertheless, the EQL distribution provides the most favorable overall fit according to the reported information criteria and goodness-of-fit measures.

For Dataset IV, the EQL and Garhy distributions provide very close and highly competitive fits. The Garhy distribution attains a slightly lower AIC (156.6900 versus 157.3872) and BIC (158.0912 versus 160.1896) than the EQL distribution. The corresponding differences are $\Delta\text{AIC} = 0.6972$ and $\Delta\text{BIC} = 2.0984$, indicating that both models receive substantial support based on the information criteria. The goodness-of-fit statistics also indicate an excellent fit for both models. In particular, EQL has a slightly larger CvM p-value (0.99464 versus 0.99037 for Garhy), whereas Garhy has a slightly larger KS p-value (0.98981 versus 0.98615 for EQL). Thus, the two models exhibit highly competitive performance for Dataset IV. Importantly, the EQL distribution remains competitive with the other considered lifetime models, including the Power Lindley, Weibull, Exponentiated-Rayleigh, and XGamma distributions.

Overall, the results provide empirical evidence that the proposed EQL distribution offers superior or highly competitive performance across the four datasets considered. It provides the best overall fit in three datasets and remains highly competitive with the best-performing alternative, Garhy, in the fourth dataset. These findings highlight the usefulness and flexibility of the proposed EQL model for analyzing lifetime data with varying degrees of skewness and variability.

Figure 4 illustrates the agreement between the empirical distributions and the fitted EQL densities. The proposed model closely represents the observed distributions across all four applications, capturing their right-skewed behavior and tail characteristics. Beyond the AIC, BIC, KS, and CvM statistics, the fitted density, CDF, survival, Q–Q, and P–P plots were examined for each dataset (Supplementary Figures S7–S10) to assess fit quality, particularly in the tails.

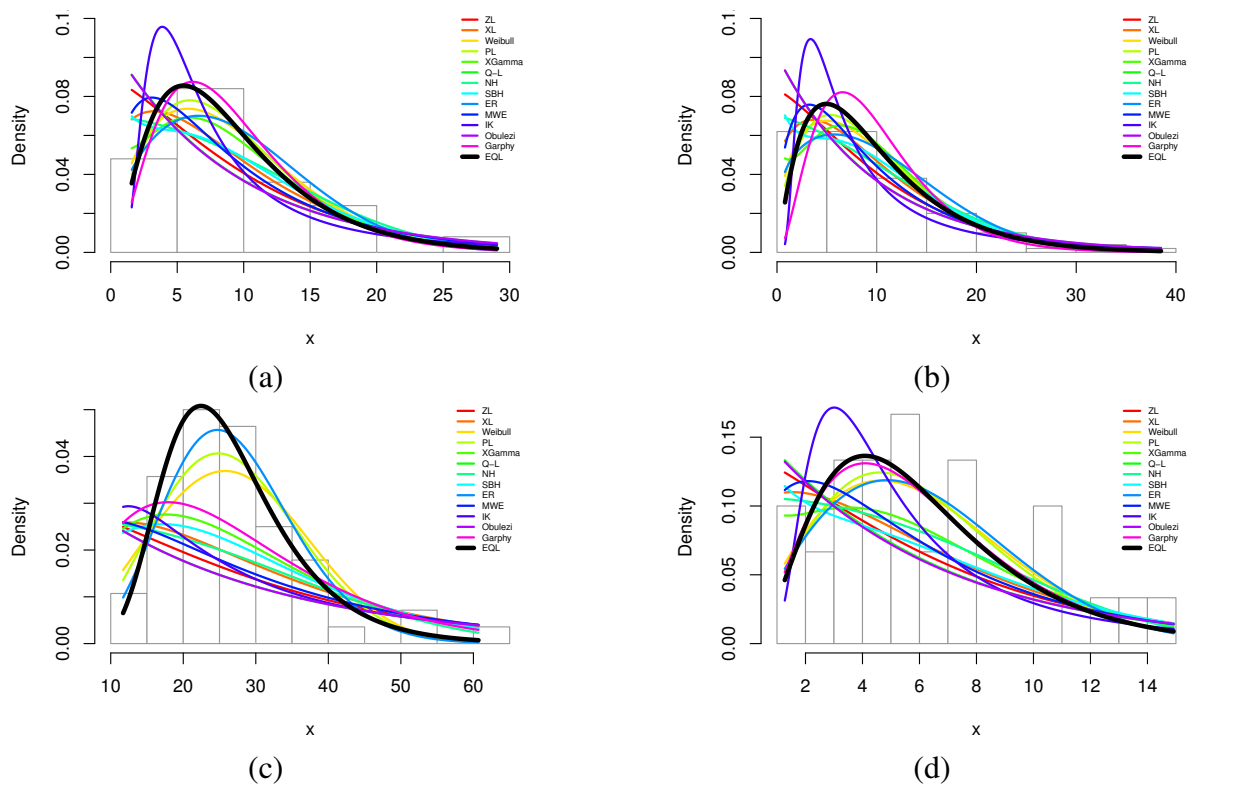


Figure 4. Histograms and fitted EQL densities for (a) Dataset I, (b) Dataset II, (c) Dataset III, and (d) Dataset IV.

For Dataset I, the CDF and survival curves closely track their empirical counterparts, and the Q–Q plot agrees well with the reference line, except for a mild deviation at the one or two largest observations, indicating a slight underestimation of the most extreme value; the P–P plot shows no comparable deviation, confirming this is confined to the extreme upper tail. For Dataset II, all four plots show close agreement with no systematic deviation, consistent with its larger sample size. The improvement over competing models here reflects EQL's ability to jointly capture the central tendency and dispersion of the data without the tail sensitivity shown by the simpler alternatives. For Dataset III, the Q–Q and P–P points lie almost exactly on the reference line throughout, including the tail, consistent with the particularly strong numerical improvement of EQL for this dataset and indicating that the extra shape parameter captures genuine structure i.e moderate right skew combined with a few elevated SO_2 readings rather than a marginal numerical gain. For Dataset IV, the diagnostics again show close agreement with no systematic deviation, consistent with the earlier finding that the EQL model describes this dataset adequately.

Profile likelihood plots for all datasets are provided in Section S6.4 of the Supplementary Material. In addition, Section S6.5 presents the results for the alternative estimation methods, whereas Section S6.6 summarizes the bootstrap confidence intervals for the four applications.

7.3. Bayesian inference

To complement the maximum likelihood analysis, Bayesian inference was conducted for the EQL distribution using the prior specification described in Section 5. Table 6 reports the posterior estimates,

minimum Bayesian risk (MBR), and 95% credible intervals for α and θ.

Table 6. Bayesian estimates, minimum Bayesian risk, and 95% credible intervals for the EQL model.

	Dataset I			Dataset II		
Parameter	Estimate	MBR	95% CI	Estimate	MBR	95% CI
α	2.6213	0.3333	(1.6335,3.9052)	2.0877	0.1065	(1.5134,2.7801)
θ	0.2150	0.0012	(0.1499,0.2881)	0.1777	0.0004	(0.1364,0.2228)
	Dataset III			Dataset IV		
Parameter	Estimate	MBR	95% CI	Estimate	MBR	95% CI
α	19.0276	43.5262	(9.6178,34.1926)	3.1303	0.8393	(1.6840,5.2183)
θ	0.1453	0.0003	(0.1129,0.1817)	0.3735	0.0054	(0.2361,0.5285)

The Bayesian estimates are broadly consistent with the corresponding maximum likelihood estimates, with the posterior intervals providing a complementary assessment of parameter uncertainty. The 95% credible intervals are finite for both parameters across all four datasets. Figure 5 presents the trace plots of α and θ for the four datasets. The chains fluctuate around stable regions without visible trends or prolonged departures from their central regions, supporting satisfactory mixing. The posterior density estimates are presented in Figure 6. The posterior distributions are unimodal and concentrated around their corresponding posterior estimates. The corresponding joint posterior contour plots and Gelman–Rubin convergence diagnostics, together with complete posterior summaries and goodness-of-fit measures, are provided in Section S6.7 of the Supplementary Material.

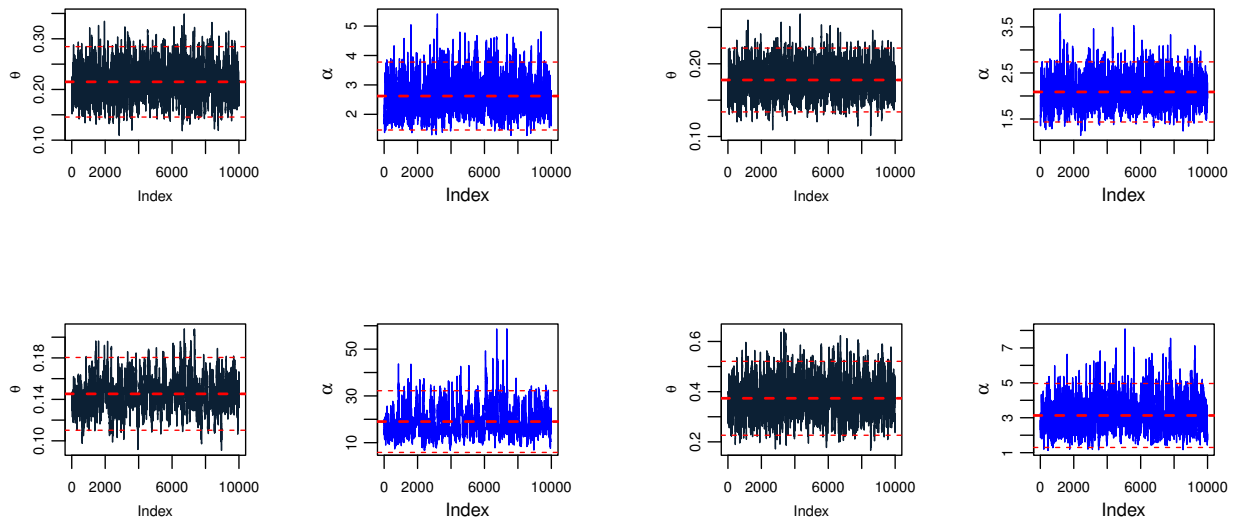


Figure 5. MCMC trace plots for α and θ for the four datasets. Datasets I and II are shown in the top row and Datasets III and IV in the bottom row.

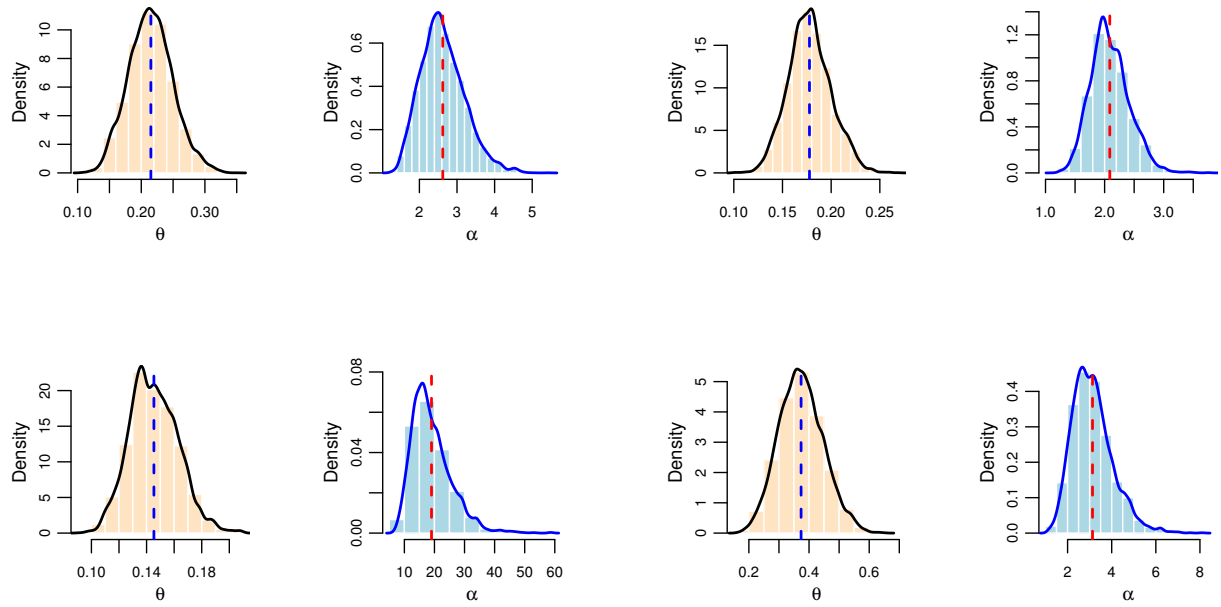


Figure 6. Posterior density plots for α and θ for the four datasets.

7.4. Likelihood ratio test

An additional assessment of the contribution of the shape parameter α is obtained by considering the Q-Lindley distribution as a nested submodel of EQL. Specifically, setting $\alpha = 1$ in the EQL model yields the Q-Lindley distribution. We therefore consider the hypotheses

$$H_0 : \alpha = 1 \qquad \text{versus} \qquad H_1 : \alpha \neq 1.$$

The likelihood ratio statistics for Datasets I–IV are 18.3473, 23.2662, 81.3482, and 15.1257, respectively, with all corresponding p-values < 0.00001. Thus, we strongly reject the null hypothesis for all four datasets. This provides additional evidence that the shape parameter α contributes significantly to model fit and that its inclusion significantly improves the simpler Q-Lindley specification.

Overall, the empirical analyses consistently support the flexibility of the EQL distribution. Under maximum likelihood estimation, EQL provides the best fit among the considered competing models according to the reported information criteria and goodness-of-fit statistics. The Bayesian analysis yields compatible parameter estimates and finite credible intervals, while the likelihood ratio tests provide formal evidence that the additional shape parameter is important in all four applications. Taken together, these results demonstrate the potential of the EQL distribution as a flexible model for positive, right-skewed data.

8. Conclusions

In this study, we introduced and investigated the exponentiated QLindley (EQL) distribution as a flexible extension of the QLindley model. By incorporating an additional shape parameter α through

exponentiation, the proposed model extends the flexibility of the QLindley distribution while retaining a tractable parametric structure. We derived several mathematical properties of the EQL distribution, including its quantile function, moments, incomplete moments, and related distributional characteristics. In addition, a comprehensive study of its reliability properties was presented, including entropy, mean inactivity time, mean residual life, reliability aging intensity, stress–strength reliability, and fuzzy reliability. Several actuarial risk measures, including the loss elimination value (LEV), value-at-risk (VaR), tail value-at-risk (TVaR), tail value (TV), and expected shortfall (ES), were also investigated.

For parameter estimation, a broad range of classical estimation methods was considered, including maximum likelihood (ML), maximum product of spacings (MPS), ordinary least squares (OLS), weighted least squares (WLS), Cramér–von Mises (CvM), Anderson–Darling (AD), and minimum spacing absolute distance (MSAD). In addition, we developed a Bayesian estimation framework based on independent gamma priors, with posterior inference performed using a Metropolis–Hastings within Gibbs algorithm. The Monte Carlo simulation study showed that the estimation performance generally improves as the sample size increases. The relative performance of the classical estimators depends on both the parameter configuration and the sample size. In particular, ML and AD provide consistently competitive results across the considered scenarios, whereas MPS performs particularly well for some parameter configurations. The Bayesian estimator also shows competitive finite-sample performance, with relatively small MSE values in several small- and moderate-sample settings.

We illustrated the practical usefulness of the EQL distribution using four real datasets from different application areas: reliability, service systems, environmental assessment, and COVID-19 mortality. Across all four datasets, the EQL model showed highly competitive performance among the considered distributions, with information criteria and goodness-of-fit statistics comparable to those of the leading competing models. The corresponding graphical diagnostics further supported the adequacy of the proposed model in capturing important features of the observed data, including skewness and tail behavior. The Bayesian analysis also provided parameter estimates broadly consistent with the maximum likelihood results, with finite 95% credible intervals for both model parameters in all four applications.

Finally, we used a likelihood ratio test to formally assess the contribution of the additional shape parameter α, using the Q-Lindley distribution as a nested submodel of the EQL distribution through $\alpha = 1$. For all four datasets, the null hypothesis $H_0 : \alpha = 1$ was strongly rejected, providing empirical evidence that the additional shape parameter leads to a significant improvement in model fit. These results also indicate that the flexibility introduced by the EQL extension is relevant in practice and is not merely a consequence of introducing an additional parameter.

Overall, the results demonstrate that the EQL distribution constitutes a useful extension of the QLindley family for modeling positive and right-skewed data. Its additional shape parameter provides greater modeling flexibility, while including the QLindley distribution as the special case $\alpha = 1$ allows the adequacy of the extension to be formally assessed. The simulation study indicates that the proposed estimation procedures perform satisfactorily across a range of sample sizes and parameter configurations, while the empirical applications demonstrate the practical advantages of the EQL model over a broad collection of competing distributions. The combination of tractable distributional properties, multiple estimation procedures, and favorable empirical performance makes the EQL distribution a promising alternative for applications involving positive and skewed data.

Author contributions

Conceptualization, P. J. H. and A. C.; investigation, S. H.; methodology, S. H., P. J. H., A. C. and D. I. G.; software, S. H.; formal analysis, S. H.; visualization, S. H.; writing–original draft preparation, S. H., P. J. H. and A. C.; writing–review and editing, D. I. G.; supervision, P. J. H. and A. C. All authors have read and agreed to the published version of the manuscript.

Use of Generative-AI tools declaration

During the preparation of this manuscript, the authors used ChatGPT (OpenAI) to assist with language editing, grammar checking, and improving clarity and readability. ChatGPT was not used to generate original research results, conduct statistical analyses, generate data, or draw scientific conclusions. The authors critically reviewed and edited all AI-assisted outputs and take full responsibility for the final content of the manuscript.

Conflict of interest

The authors have no relevant financial or non-financial interests to disclose.

References

1. N. Eugene, C. Lee, F. Famoye, Beta-normal distribution and its applications, *Commun. Stat. Theory Methods*, **31** (2002), 497–512. https://doi.org/10.1081/STA-120003130
2. M. Bourguignon, R. B. Silva, G. M. Cordeiro, The Weibull-G family of probability distributions, *J. Data Sci.*, **12** (2014), 53–68. https://doi.org/10.6339/JDS.2014.12(1).1210
3. S. A. Lone, T. N. Sindhu, A. Shafiq, F. Jarad, A novel extended Gumbel Type II model with statistical inference and Covid-19 applications, *Results Phys.*, **35** (2022), 105377. https://doi.org/10.1016/j.rinp.2022.105377
4. J. T. Eghwerido, L. C. Nzei, A. E. Omotoye, F. I. Agu, The Teissier-G family of distributions: properties and applications, *Math. Slovaca*, **72** (2022), 1301–1318. https://doi.org/10.1515/ms-2022-0089
5. O. H. Odhah, H. M. Alshanbari, Z. Ahmad, G. S. Rao, A weighted cosine-G family of distributions: properties and illustration using time-to-event data, *Axioms*, **12** (2023), 849. https://doi.org/10.3390/axioms12090849
6. H. Al-Mofleh, M. Elgarhy, A. Afify, M. Zannon, Type II exponentiated half logistic generated family of distributions with applications, *Electron. J. Appl. Stat. Anal.*, **13** (2020), 536–561. https://doi.org/10.1285/i20705948v13n2p536
7. S. M. Alghamdi, M. Shrahili, A. S. Hassan, R. E. Mohamed, I. Elbatal, M. Elgarhy, Analysis of milk production and failure data: using unit exponentiated half logistic power series class of distributions, *Symmetry*, **15** (2023), 714. https://doi.org/10.3390/sym15030714

8. M. A. Aldahlan, F. Jamal, C. Chesneau, I. Elbatal, M. Elgarhy, Exponentiated power generalized Weibull power series family of distributions: properties, estimation and applications, *PLoS One*, **15** (2020), e0230004. https://doi.org/10.1371/journal.pone.0230004

9. A. Ahmad, A. Ahmad, Y. A. Tashkandy, M. E. Bakr, G. T. Mekiso, O. S. Balogun, et al., A study on the new logarithmic-G family with statistical properties, simulations, and different data analysis, *Sci. Rep.*, **15** (2025), 15069. https://doi.org/10.1038/s41598-025-99525-4

10. S. Zacks, Estimating the shift to wear-out of systems having exponential-Weibull life distributions, *Oper. Res.*, **32** (1984), 741–749. https://doi.org/10.1287/opre.32.3.741

11. G. S. Mudholkar, D. K. Srivastava, Exponentiated Weibull family for analyzing bathtub failure-rate data, *IEEE Trans. Reliab.*, **42** (1993), 299–302. https://doi.org/10.1109/24.229504

12. S. A. Lone, Q. Ramzan, L. A. AL-Essa, The exponentiated Ailamujia distribution: properties and application, *Alexandria Eng. J.*, **108** (2024), 1–15. https://doi.org/10.1016/j.aej.2024.09.036

13. S. Nadarajah, S. Kotz, The exponentiated Fréchet distribution, *Interstat Electron. J.*, **14** (2003), 01–07.

14. S. Nadarajah, The exponentiated Gumbel distribution with climate application, *Environmetrics*, **17** (2006), 13–23. https://doi.org/10.1002/env.739

15. S. Nadarajah, H. S. Bakouch, R. Tahmasbi, A generalized Lindley distribution, *Sankhya B*, **73** (2011), 331–359. https://doi.org/10.1007/s13571-011-0025-9

16. M. Nassar, S. Dey, D. Kumar, A new generalization of the exponentiated Pareto distribution with an application, *Am. J. Math. Manag. Sci.*, **37** (2018), 217–242. https://doi.org/10.1080/01966324.2017.1396942

17. H. M. Salem, The exponentiated Lomax distribution: different estimation methods, *Am. J. Appl. Math. Stat.*, **2** (2014), 364–368. https://doi.org/10.12691/ajams-2-6-2

18. B. Peng, Z. Xu, M. Wang, The exponentiated Lindley geometric distribution with applications, *Entropy*, **21** (2019), 510. https://doi.org/10.3390/e21050510

19. A. M. Alomair, M. Ahmed, S. Tariq, M. Ahsan-ul-Haq, J. Talib, An exponentiated XLindley distribution with properties, inference and applications, *Heliyon*, **10** (2024), e25472. https://doi.org/10.1016/j.heliyon.2024.e25472

20. S. M. T. K. MirMostafaee, The exponentiated new XLindley distribution: properties and applications, *J. Data Sci. Model.*, **2** (2024), 185–208. https://doi.org/10.22054/jdsm.2024.81152.1051

21. E. S. Alotaibi, An exponentiated ZLindley distribution with application to breast cancer and radiotherapy data, *J. Radiat. Res. Appl. Sci.*, **18** (2025), 101755. https://doi.org/10.1016/j.jrras.2025.101755

22. A. M. Sarhan, A. S. M. Al Luhayb, R. Alotaibi, M. E. Sobh, The exponentiated modified Lindley distribution with diverse biomedical and epidemiological applications, *AIMS Math.*, **11** (2026), 2313–2340. https://doi.org/10.3934/math.2026093

23. N. Saaidia, R. Pakyari, H. Zeghdoudi, The Q-Lindley distribution: goodness-of-fit tests, modeling, inference, and applications, *J. Stat. Theory Appl.*, **25** (2026), 6. https://doi.org/10.1007/s44199-025-00148-5

24. R. Elbarougy, J. Das, P. J. Hazarika, M. S. Eliwa, The bimodal two-piece skew-normal distribution: mathematical theory, reliability aging measures, and simulation-oriented decision analysis, *AIMS Math.*, **11** (2026), 511–542. https://doi.org/10.3934/math.2026022

25. R. Jiang, P. Ji, X. Xiao, Aging property of unimodal failure rate models, *Reliab. Eng. Syst. Saf.*, **79** (2003), 113–116. https://doi.org/10.1016/S0951-8320(02)00175-8

26. B. Efron, Bootstrap methods: another look at the jackknife, In: *Breakthroughs in statistics: methodology and distribution*, New York: Springer, 1992. https://doi.org/10.1007/978-1-4612-4380-9_41

27. M. E. Ghitany, D. K. Al-Mutairi, N. Balakrishnan, L. J. Al-Enezi, Power Lindley distribution and associated inference, *Comput. Stat. Data Anal.*, **64** (2013), 20–33. https://doi.org/10.1016/j.csda.2013.02.026

28. S. Sen, S. S. Maiti, N. Chandra, The xgamma distribution: statistical properties and application, *J. Mod. Appl. Stat. Methods*, **15** (2016), 38. https://doi.org/10.22237/jmasm/1462077420

29. C. Chesneau, V. Kumar, M. Khetan, M. Arshad, On a modified weighted exponential distribution with applications, *Math. Comput. Appl.*, **27** (2022), 17. https://doi.org/10.3390/mca27010017

30. M. G. M. Ghazal, H. M. Hasaballah, Exponentiated rayleigh distribution: a Bayes study using MCMC approach based on unified hybrid censored data, *J. Adv. Math.*, **12** (2017), 6863–6880.

31. S. Chouia, H. Zeghdoudi, The XLindley distribution: properties and application, *J. Stat. Theory Appl.*, **20** (2021), 318–327. https://doi.org/10.2991/jsta.d.210607.001

32. M. Elgarhy, Garhy distribution with different estimation methods and applications to engineering and medical data, *Rev. Int. Métodos Numér. Cálc. Diseño Ing.*, **42** (2026), 90. Available from: `https://www.scipedia.com/public/Elgarhy_2026a`

33. O. J. Obulezi, Obulezi distribution: a novel one-parameter distribution for lifetime data modeling, *Mod. J. Stat.*, **2** (2025), 32–74. https://doi.org/10.64389/mjs.2026.02140

34. H. A. Khogeer, An improved one-parameter weighted distribution with mathematical properties, estimation, and applications, *Alex. Eng. J.*, **104** (2024), 222–234. https://doi.org/10.1016/j.aej.2024.06.005

35. A. M. Abd Al-Fattah, A. A. El-Helbawy, G. R. Al-Dayian, Inverted Kumaraswamy distribution: properties and estimation, *Pak. J. Statist.*, **33** (2017), 37–61.

36. S. Nadarajah, F. Haghighi, An extension of the exponential distribution, *Statistics*, **45** (2011), 543–558. https://doi.org/10.1080/02331881003678678

37. D. N. P. Murthy, M. Xie, R. Jiang, *Weibull models*, New York: John Wiley & Sons, 2004. https://doi.org/10.1002/047147326X

38. M. E. Ghitany, B. Atieh, S. Nadarajah, Lindley distribution and its application, *Math. Comput. Simul.*, **78** (2008), 493–506. https://doi.org/10.1016/j.matcom.2007.06.007

39. H. M. Almongy, E. M. Almetwally, H. M. Aljohani, A. S. Alghamdi, E. H. Hafez, A new extended Rayleigh distribution with applications of COVID-19 data, *Results Phys.*, **23** (2021), 104012. https://doi.org/10.1016/j.rinp.2021.104012

Appendix

The datasets used in this study are available in the associated GitHub repository. `https://github.com/sajadulhussain/EQL-Model.git`



© 2026 the Author(s), licensee AIMS Press. This is an open access article distributed under the terms of the Creative Commons Attribution License (https://creativecommons.org/licenses/by/4.0)